frontiers in Earth Science

REVIEW
published: 12 April 2021
doi: 10.3389/feart.2021.668566

Monazite Microstructures and Their Interpretation in Petrochronology

*Bernhard Schulz**

Division of Economic Geology and Petrology, Institute of Mineralogy, Freiberg University of Mining and Technology, Freiberg/Saxony, Germany

The phosphate mineral monazite (LREE,Y,Th,Ca,Si)PO_4 occurs as an accessory phase in peraluminous granites and Ca-poor meta-psammopelites. Due to negligible common Pb and very low Pb diffusion rates at high temperatures, monazite has received increasing attention in geochronology. As the monazite grain sizes are mostly below 100 μm in upper greenschist to amphibolite facies meta-psammopelites, and rarely exceed 250 μm in granulite facies gneisses and in migmatites, microstructural observation and mineral chemical analysis need the investigation by scanning electron microscope and electron probe microanalyzer, with related routines of automated mineralogy. Not only the microstructural positions, sizes and contours of the grains, but also their internal structures in backscattered electron imaging gray tones, mainly controlled by the Th contents, can be assessed by this approach. Monazite crystallizes mostly euhedral to anhedral with more or less rounded crystal corners. There are transitions from elliptical over amoeboid to strongly emarginated grain shapes. The internal structures of the grains range from single to complex concentric over systematic oszillatory zonations to turbulent and cloudy, all with low to high contrast in backscattered electron imaging gray tones. Fluid-mediated partial alteration and coupled dissolution-reprecipitation can lead to Th-poor and Th-rich rim zones with sharp concave boundaries extending to the interior. Of particular interest is the corona structure with monazite surrounded by apatite and allanite, which is interpreted to result from a replacement during retrogression. The satellite structure with an atoll-like arrangement of small monazites may indicate re-heating after retrogression. Cluster structures with numerous small monazite grains, various aggregation structures and coating suggest nucleation and growth along heating or/and enhanced fluid activity. Microstructures of monazite fluid-mediated alteration, decomposition and replacement are strongly sutured grain boundaries and sponge-like porosity and intergrowth with apatite. Garnet-bearing assemblages allow an independent reconstruction of the pressure-temperature evolution in monazite-bearing meta-psammopelites. This provides additional potential for evaluation of the monazite microstructures, mineral chemistry and Th-U-Pb ages in terms of clockwise and counterclockwise pressure-temperature-time-deformation paths of anatectic melting, metamorphism and polymetamorphism. That way, monazite microstructures serve as unique indicators of tectonic and geodynamic scenarios.

Keywords: monazite, meta-psammopelites, peraluminous granites, dissolution-reprecipitation, corona microstructure, satellite microstructure, P-T-time-deformation paths

OPEN ACCESS

Edited by:
Sebastian Oriolo, Consejo Nacional de Investigaciones Científicas y Técnicas (CONICET), Argentina

Reviewed by:
Junpeng Wang, China University of Geosciences Wuhan, China
Sergio Llana-Fúnez, University of Oviedo, Spain

***Correspondence:**
Bernhard Schulz
bernhard.schulz@mineral.tu-freiberg.de

Specialty section:
This article was submitted to Structural Geology and Tectonics, a section of the journal Frontiers in Earth Science

Received: *16 February 2021*
Accepted: *23 March 2021*
Published: *12 April 2021*

Citation:
Schulz B (2021) Monazite Microstructures and Their Interpretation in Petrochronology. Front. Earth Sci. 9:668566. doi: 10.3389/feart.2021.668566

INTRODUCTION

The phosphate mineral monazite (LREE,Th,Y,Si,Ca)PO_4 - first described by Breithaupt (1829) in Freiberg/Saxony - is an igneous accessory phase in peraluminous granites, syenite, and granitic pegmatites, quartz veins, and carbonatites. It is also common as an accessory mineral in metapelitic rocks with Ca-poor and Al-rich bulk compositions at all metamorphic grades above the upper greenschist facies. Monazite occurs in low-pressure contact metamorphic rocks, in high-grade garnet cordierite K-feldspar gneisses, in granulites, migmatites, charnockites and also in coesite-bearing ultra high pressure garnet gneisses (e.g., Overstreet, 1967; Spear and Pyle, 2002; Brandt et al., 2011; Petrík et al., 2019). However, monazite is not an approved high pressure phase and apparently crystallizes prior to and/or after to the peak pressures. Monazite is also observed in connection with hydrothermal and metasomatic ore deposits (e.g., Poitrasson et al., 1996; Hecht and Cuney, 2000; Schandl and Gorton, 2004; Kempe et al., 2008; Janots et al., 2012; Seydoux-Guillaume et al., 2012). Such a genetic association with crustal fluids encouraged petrologic experiments in order to understand monazite formation, its behavior in nature and the consequences for age dating, especially in terms of dissolution-reprecipitation (e.g., Harlov and Förster, 2003; Harlov et al., 2005, 2011; Hetherington et al., 2010; Budzyń et al., 2011, 2017).

Monazite has variable mineral chemical compositions. Its nominal composition is dominated by La, Ce, and Nd which together comprise 2.8 - 3.2 cations per 4 oxygen (per formula unit p.f.u) of the total cation proportions. The other REE such as Pr, Sm, Eu and Gd, occur in minor proportions (0.3 - 0.4 cations p.f.u.). Most monazites contain additional Ca, Si and HREE at concentrations less than 0.02 cations p.f.u., but Y concentrations can reach up to 0.1 cations p.f.u. (e.g., Quarton et al., 1994; Franz et al., 1996; Gratz and Heinrich, 1997; Heinrich et al., 1997; Förster, 1998; Zhu and O'Nions, 1999; Spear and Pyle, 2002; Linthout, 2007). The Th occurs in igneous and metamorphic monazite with up to 0.25 cations p.f.u., but most metamorphic monazite has less than 0.05 Th p.f.u. The U concentrations are comparably low and range from 0.01 - 0.005 cations (p.f.u.). Apart from the monazite - xenotime exchange Y = REE, the Th + Si = REE + P (huttonite) exchange and the Th + Ca = 2REE (cheralite) exchange can operate. As a consequence of the mineral-chemical variability, there are numerous reports of compositional zoning in igneous and metamorphic monazite (Spear and Pyle, 2002 and references therein).

The mineral chemical and crystallographic characteristics of monazite made it a perfect target for *in situ* geochronology besides the classical U-Pb isotope measurements by TIMS, SIMS and LA-MC-ICP-MS (e.g., Harrison et al., 2002). *In situ* monazite Th-U-Pb dating by the electron probe microanalyser (EPMA) is based on the observation that common Pb in monazite is negligible when compared to radiogenic Pb resulting from the decay of Th and U (e.g., Parrish, 1990; Montel et al., 1996; Braun et al., 1998; Cocherie et al., 2005). Also, monazite shows extremely low diffusion rates for the radiogenic Pb at high temperatures. Cherniak et al. (2004) reported that a 10-μm-sized monazite grain would have a Pb closure temperature in excess of 900°C, given a cooling rate of 10°C/Ma. Apparently, the Pb is fixed in the monazite structure, which explains the low tendency of this element to escape from monazite. Also it is generally agreed that radiation damage in monazite self-anneals over geological periods of time even at relatively low temperatures, thus preventing the accumulation of significant amounts of damage (e.g., Meldrum et al., 1998; Nasdala et al., 2018). Therefore, EPMA analysis of the bulk Th, U, and Pb concentrations in monazite, at a constant $^{238}U/^{235}U$, allows for the calculation of an isochron age (Suzuki and Adachi, 1991; Suzuki and Kato, 2008) and/or for single domain ages with a considerable error (e.g., Montel et al., 1996; Pyle et al., 2005; Jercinovic et al., 2008; Spear et al., 2009; Williams et al., 2017; Montel et al., 2018). The younger age limit of the EPMA Th-U-Pb monazite dating method is at about 100 Ma, as given by the detection limit for Pb (Montel et al., 1996). For the monazite U-Pb dating methods by isotope ratio measurement with SIMS and LA-ICP-MS the younger age limits are considerable lower. However, these methods have also limitations, given by small monazite grain sizes and the incomplete mineral compositional data beside Th, U, and Pb.

As a consequence, monazite microstructures are not stand-alone. They are accompanied by the variable monazite mineral-chemical compositions and the *in situ* Th-U-Pb dating perspective. In combination this provides a great potential to understand the monazite genesis and gives irreplaceable petrochronological constraints for the reconstruction of ancient orogens. This contribution provides a review of monazite microstructures and their implications for the igneous and metamorphic evolution. Monazite microstructures in different rock types and variable tectonic settings are presented, together with specific microstructures that are relevant for the understanding of petrogenetic processes. The sample locations and provenance of monazite microphotos in the figures are listed with related references as electronic supplement. The manifold analytical details of compositions and age dating procedures of the processes which lead to distinct monazite microstructures are beyond the scope of this contribution. However, there is one more interesting aspect of monazite microstructures: Monazite often occurs in garnet-bearing meta-psammopelites which allow an independent reconstruction of metamorphic P-T-time deformation paths in reference to the monazite P-T stability field. This approach is presented by reporting some case studies which include the evaluation and interpretation of the monazite microstructures in terms of the pressure-temperature evolution.

ANALYTICAL APPROACH TO MONAZITE MICROSTRUCTURES

The details of the *in situ* analysis of monazite chemical composition and the Th-U-Pb dating by EPMA, LA-ICP-MS and SIMS have been outlined and updated in numerous publications (e.g., Montel et al., 1996, 2018; Scherrer et al., 2000; Pyle et al., 2005; Jercinovic et al., 2008; Suzuki and Kato, 2008; Spear et al., 2009; Zhang et al., 2015; Ling et al., 2017; Williams et al., 2017; Richter et al., 2019; Schulz et al., 2019b). Thus, this contribution

is focussed on the evaluation of monazite microstructures, and their detection and characterization. Although monazite grain sizes of >1 mm have been reported (Spear and Pyle, 2002), the grain size of most igneous and metamorphic monazite range below 200 μm, mostly at 100 - 10 μm. Thus, for search and petrographic documentation of monazite in thin sections, the scanning electron microscope (SEM) is essential. Automated mineralogical methods (e.g., Schulz et al., 2020), based on an SEM equipped with image analysis software, an automated steering of the electron beam, and energy dispersive spectrometers for EDS analyses, can be applied to thin sections of potentially monazite-bearing rocks. Software packages for mineral liberation analysis (MLA versions 2.9 or 3.1 and QEMSCAN by FEI Company) or alternative software platforms by Zeiss Mineralogic Systems and TESCAN TIMA can then be used for the automated steerage of the electron beam for EDS identification of mineral grains and the collection of EDS spectra. Of special interest for the search for monazite are automated mineralogy routines actually designed for the detection of rare phases as gold or platinum group minerals. Such routines combine a backscattered electron (BSE) gray color value trigger and single spot EDS spectral analysis. The BSE gray color value at 25 kV acceleration voltage of the electron beam is set at 250 for gold and at 25 for the epoxy raisin at the margin of the petrographic thin section. In this gray color scale, monazite is very bright and will have a value of >120. When the BSE gray color value trigger for the search is set at >90, then monazite, xenotime, zircon, most sulfides ores, Fe- and Fe-Ti-oxides will be detected automatically. Apatite which may be also of interest has a value of ∼70 and will not be detected as a rare phase, as its BSE gray color value overlaps with biotite and garnet, and other Fe-bearing silicates (BSE gray color ∼50 - 80). For the classification of the measured minerals, a list of identified reference EDS spectra has to be collected and applied. Usually the rare phase detection routines then deliver a catalogue of false-colored images, which document grain counts and area, grain sizes and shapes, and the microstructural relationships of the monazite grains and their hosting and neighboring minerals within a distance of ∼100 μm from the margin of the target mineral (**Figure 1**). This can be used to select specific monazite grains for a direct SEM stage-drive access and for successive detailed EPMA, LA-ICP-MS and SIMS analysis. A manual search for monazite by scrolling a thin section sample under the BSE detector can also be considered.

For the detailed documentation of the monazite microstructures several steps are recommended. At normal BSE contrast and brightness the monazite grains appear with homogeneous bright and white color, whereas the neighboring minerals like feldspars, quartz, mica or garnet appear with dark to light BSE gray colors. For the resolution of the internal structures of monazite, a considerably different modulation of the BSE contrast and brightness is necessary. The contrast should be increased while brightness is decreased until the surrounding matrix minerals are completely dark and the internal structures of monazite are visible. In general, the light parts of the monazite coincide with high Th contents. After semiquantitative controls of the Th contents within the monazite grain by EDS, the contrast/brightness should be reset to verify the matrix phases by EDS, especially in reaction microstructures. The SEM automated mineralogy investigations show that monazite grain counts (500 - 30) and the grain diameters (100 - 20 μm) can vary considerably in thin sections (Schulz, 2017; Schulz et al., 2019b). Usually, the grain size at the cumulative 50 wt% of the cumulative grain size distribution curve (P50 or Md50) is reported. Depending on the abundance and grain size, a further detailed documentation of ∼20 larger grains per sample and also by additional wavelength dispersive spectroscopy element mapping is recommended. One has to be aware that monazite grain sizes and internal microstructures as observed *in situ* in petrographic thin sections may considerably differ from monazite in related heavy mineral concentrates, especially when migmatites are studied (Oyhantçabal et al., 2012; Schulz and Schüssler, 2013).

MICROSTRUCTURES OF MONAZITE

Microstructures in Igneous and Metamorphic Rocks

Microstructures of Monazite in Granitoids

Monazite occurs as an accessory mineral in muscovite-bearing peraluminous granitoids and in cordierite-bearing peraluminous granitoids, following the plausible classification of Barbarin (1998). In these "S-type" granitoids, generated by anatectic melting of crustal rocks, the abundance of monazite is classified as rare when compared to abundant apatite. In the other granitoid types with increasing share of mantle melts, the igneous and mantle granitoid types in the Barbarin (1998) classification, the monazite is generally absent. Monazite may rarely occur in metaluminous and peralkaline igneous rocks, and it is apparently abundant in carbonatites, though these rock types are not considered in this compilation. In peraluminous granites, the monazite is accompanied by apatite, zircon, xenotime, tourmaline, garnet and occasionally allanite. Monazite often displays euhedral to anhedral shapes and usually exceeds grain sizes of 100 μm, being commonly enclosed in biotite. In biotite, the pleochroitic halos around monazite in combination with platy grain shapes contrasting prismatic zircon grains with straight extinction, makes them detectable also by optical microscopy under polarized light.

The common occurrence of monazite with zircon in such granitoids (e.g., Montel, 1993; Finger et al., 2003) has been used to establish reference monazites for geochronology (EPMA-Th-U-Pb; SIMS-U-Pb; LA-ICP-MS-U-Pb), as zircon in granitoids allows an independent U-Pb dating of its crystallization age from the granitic melt, if not inherited (e.g., Ling et al., 2017; Richter et al., 2019). Monazite in granitoids can display homogeneous interior parts (**Figures 2a,b**) or weak zonations of the gray color appearance in BSE images (**Figure 2e**). In pegmatites, monazite can occur in cm-sized crystals. Parts of such large monazites can show variable Th contents and traces of alteration with tiny holes along cracks, so that domains for reference measurements should be carefully selected (**Figures 2c,d**). However, it is important to emphasize that natural reference monazites involved in the

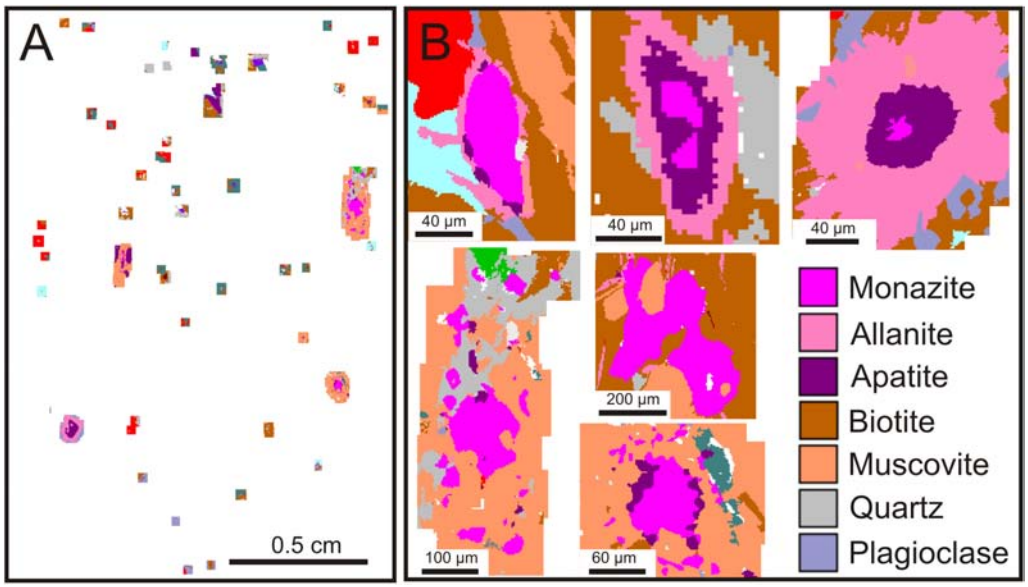

FIGURE 1 | Search for monazite by scanning electron microscopy automated mineralogy methods (e.g., Schulz et al., 2020). **(A)** Merged frame view of a rare phase search measurement routine applied to a polished thin section. **(B)** Examples of monazite and its surrounding minerals in a false-colored view as combined from backscattered electron image analysis and energy dispersive spectroscopy spectrum classification by the rare phase search routine. See text for explanation.

calibration and adjustment of the monazite Th-U-Pb SIMS and SHRIMP age dating protocols are not necessarily suitable as reference material for Th-U-Pb EPMA monazite dating (Schulz and Schüssler, 2013). Reference monazite with perfectly homogeneous BSE gray tone as VK-1 (**Figure 2b**) has a large variation in PbO at constant Th + U and is thus inadequate as reference for the Th-U-Pb EPMA dating method. The MPN monazite (**Figure 2d**) can be used under the restriction that only the unaltered domains are taken into account. Judging from its ThO_2*–PbO characteristics, monazite like the Madmon (**Figure 2c**) appears as suitable for the correlation of U-Pb isotopic and Th-U-Pb bulk chemical age dating methods, when homogeneous unaltered domains and the comparably high Th contents are considered (Schulz and Schüssler, 2013).

Euhedral monazite in granitoids display either weak and/or striking single and complex concentric (**Figures 2e,f**) or oscillatory zonations along straight boundaries of BSE gray colors (**Figures 2g,h**). Irregular cloudy and patchy BSE gray color interior domains are observed (**Figures 2h-l**), sometimes in combination with oscillatory zonation (**Figure 2h**). A close association of monazite with zircon and also with Fe-Ti minerals (**Figure 2m**) occurs in peraluminous Pan-African granitoids of Cameroon (Djouka-Fonkwe et al., 2008). Interesting are also the possible indicators of a subsolidus and post-magmatic alteration of the monazites, as small cavities and irregular fissures (**Figures 2d,f**), and sutured instead of straight grain boundaries (**Figure 2d**).

As known from zircon, needle-type monazite has been found in evolved peraluminous "Greisen" granitoids of Zinnwald (Erzgebirge). They display a patchy distribution of BSE gray colors. In some cases the needles crystallized parallel to the cleavage planes of mica and can also be enclosed by quartz (**Figures 2n,o**). They are interpreted to have crystallized during the greisenization when fluids entered during the later subsolidus stages of granite cooling (Johan and Johan, 2005; Ondrejka et al., 2007, 2009). In the same samples from the Zinnwald greisen granite, small monazite (<10 µm) with irregular grain shapes occur in fluorite. These examples demonstrate that monazite potentially crystallizes also during the post-magmatic evolution of granitoids, particularly when associated with late fluids.

Monazite in High-Grade Metamorphic Rocks

High-grade metamorphic aluminous garnet gneisses, sometimes labelled also as kinzigites are of special interest for metamorphic studies, as they allow P-T path reconstruction by geothermobarometric methods in combination with EPMA, LA-ICP-MS and SIMS Th-U-Pb monazite dating (e.g., Audren and Triboulet, 1993; Schulz, 2013; Schulz and Krause, 2018). Monazite in high-grade aluminous gneisses, mostly display anhedral elliptical to amoeboid and well-rounded grain shapes. Grain sizes can reach up to several 100 µm. As intragranular features one observes mostly weak variations of patchy areas of BSE gray colors which appear sometimes in combination with zonations (e.g., Braun et al., 1998; Simmat and Raith, 2008; Brandt et al., 2011). No significant differences in grain shapes and internal structures between monazites from the intermediate pressure cordierite-garnet gneisses (kinzigites) from the Saxonian Granulite Massif and other metamorphic terrains (**Figures 3a-c**) and ultra high pressure garnet gneisses from the Central Erzgebirge (**Figures 3d,e**) have been observed (Tichomirowa et al., 2018; Schulz et al., 2019a). When monazite crystallizes in domains with fibrolithic sillimanite as in the cordierite-garnet gneisses, then numerous inclusions of sillimanite needles are

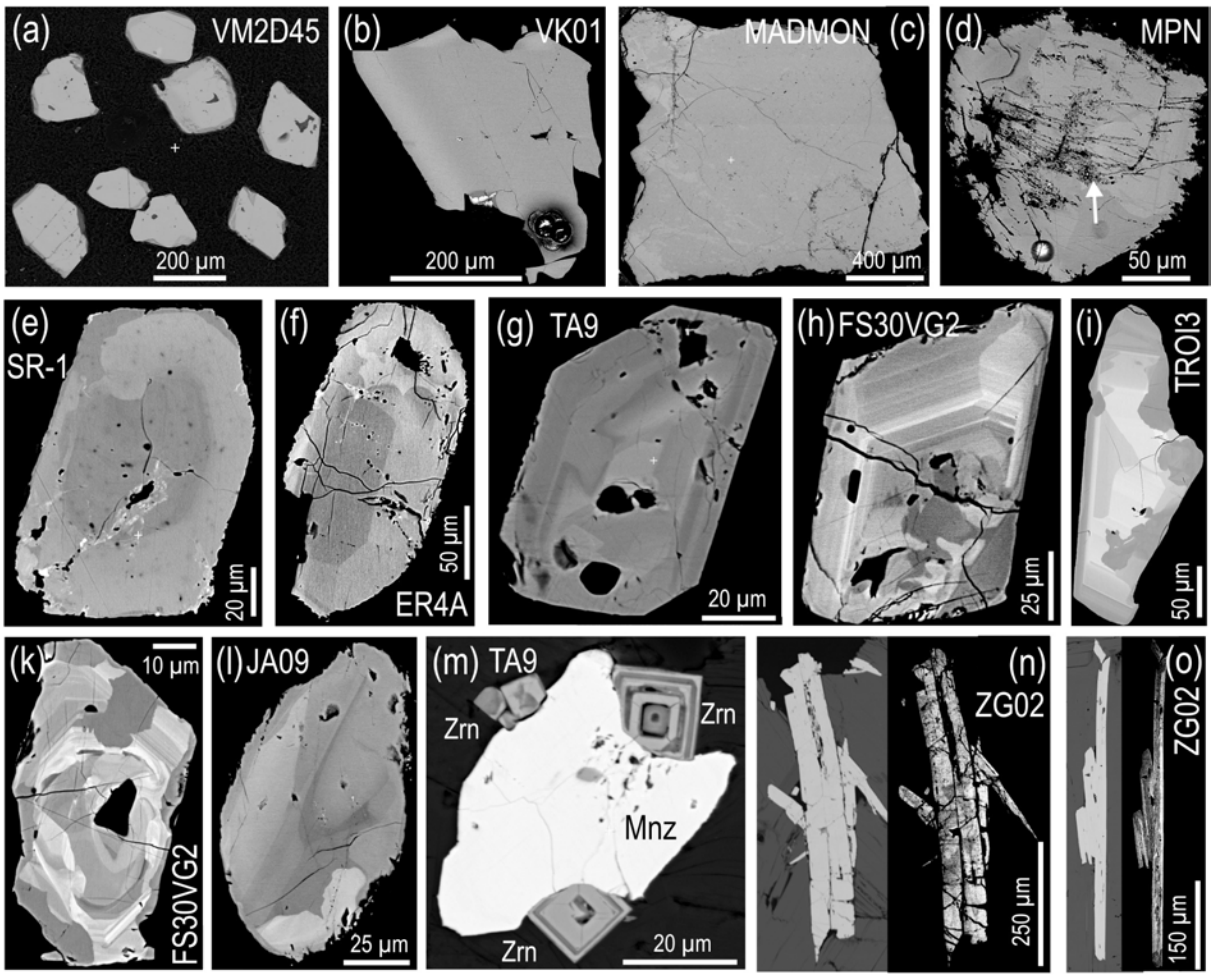

FIGURE 2 | Monazite in peraluminous granite and pegmatite. **(a)** Euhedral monazite from a granite in a grain mount, distributed as a reference material for EPMA Th-U-Pb age dating by BRGM Orléans. **(b)** Inclusion-free monazite with perfect homogeneous distribution of Th from a granite, used as reference material for U-Pb SHRIMP monazite dating. **(c)** Reference monazite from a Madagascar pegmatite, with cracks separating homogeneous domains (Schulz and Schüssler, 2013). **(d)** Reference monazite with sutured grain boundary, numerous cracks and domains of alteration (arrow), used as reference material for SHRIMP U-Pb monazite dating. **(e,f)** Euhedral large monazite with cracks and zoned distribution of Th in Erinpura granitoid (Just et al., 2010). **(g)** Euhedral zoned monazite from a Pan-African two-mica granite (Djouka-Fonkwe et al., 2008). **(h,i)** Monazite with symmetric zonation of the margin and amoeboid distribution of Th in the core, from Mittweida granite and Troischau granite dike, Saxonian Granulite Massif. **(k)** Monazite with cloudy or amoeboid internal distribution of Th from Mittweida granite. **(l)** Paleoproterozoic monazite with embayment of a Th-rich marginal zone from a granite in the Ntem Unit (Cameroon). **(m)** Monazite with contact to several zircon (Zrn) crystals in a Pan-African granite. **(n,o)** Needle-shaped euhedral monazite from the Zinnwald greisen granite (Erzgebirge).

obvious (**Figure 3f**). Such observations of inclusions may serve for an interpretation of the monazite ages in the metamorphic crystallization-deformation sequence.

Monazite in migmatites can display marked light Th-rich (**Figure 3g**) as well as dark Th-poor marginal domains (**Figure 3h**). Some large monazites in the grain mounts from the Wilson Terrane (Antarctica) display structures of dark embayments into light domains in BSE images (**Figure 3h**). The dark domains have lower ThO_2 (<9 wt%) and lower SiO_2 and UO_2, but higher Ce_2O_3 and P_2O_5 when compared to the light domains (Schulz and Schüssler, 2013). Similar mineral-chemical trends and structures have been described from monazites which were experimentally metasomatised by alkali-bearing fluids (e.g., Harlov et al., 2011; Williams et al., 2011). Th-rich zones with light BSE gray tones and convex inward curved boundaries were observed in grain mounts of large monazites in Paleoproterozoic granulites from Uruguay (Oyhantçabal et al., 2012). Other monazite grains of the same grain mount show patchy domains with marked dark and light BSE gray tone contrast (**Figures 3i-l**). There are also monazite with colloidal zonations with partial internal and/or marginal dissolution (**Figures 3m,n**). These features appear in rocks which underwent a post-granulitic metamorphic overprint at amphibolite-facies conditions. When zircon and monazite ages from such overprinted high-grade Paleoproterozoic areas are compared (Oyhantçabal et al., 2012), the monazite signals an about 50 - 100 million years younger event. However, zircon and monazite may display different age response

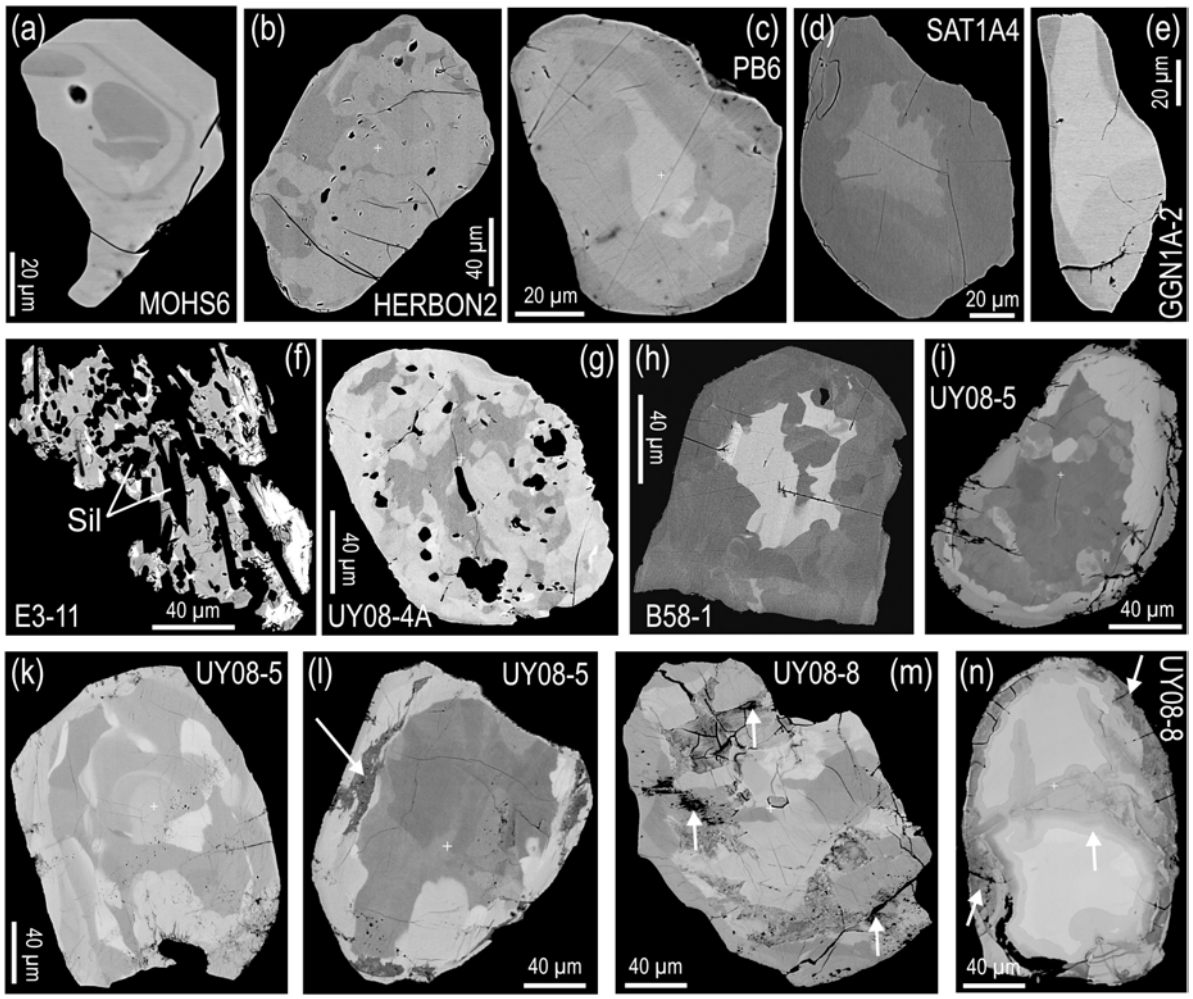

FIGURE 3 | Monazite in high-grade garnet gneiss and migmatite. **(a)** Weakly zoned and partly euhedral monazite in cordierite garnet gneiss ("kinzigite") from the Saxonian Granulite Massif. **(b)** Euhedral monazite with cloudy internal domains and rounded corners from cordierite garnet gneiss (Schulz, 2013). **(c)** Monazite with rounded corners from a garnet gneiss in the Wilson Terrane, Antarctica (Schulz and Schüssler, 2013). **(d,e)** Poorly zoned monazite in UHP garnet gneiss ("saidenbachite") from the Central Erzgebirge (Tichomirowa et al., 2018). **(f)** Monazite with numerous inclusions of decussate prismatic sillimanite in cordierite garnet gneiss (Saxonian Granulite Massif). **(g)** Monazite with bright margin and cloudy internal domains from Isla Cristalina de Rivera, Uruguay (Oyhantçabal et al., 2012). **(h)** Monazite with dark Th-poor margin from a diatexite in the Wilson Terrane. **(i-n)** Monazites with lobate marginal zones, alteration zones and increasing grade of alteration (arrows) in a grain mount from Isla Cristalina de Rivera, Uruguay.

at such high-grade metamorphic events (Zeh et al., 2003; Kelsey et al., 2008).

The microstructures of monazites in contact to granitic melts were studied in experiments by Varga et al. (2020). In nature, such a case could be when granites are re-melted during overprint by granulite facies metamorphism or when a regional high-grade metamorphic event leads to partial anatexis and migmatization. In the experiments (Varga et al., 2020), several distinct zones T1 to T4 are developed when monazite gets into contact to a melt: Zone T1 is a relict precursor monazite preserved in core domains of grain fragments that is brighter in BSE response and visually lacking discernible reaction textures. Zone T2 is monazite with fine melt-filled porosity (1–2 µm) that is spatially restricted to the margins of T1 and shows similar BSE brightness. The zone T3 is monazite with coarser melt-filled porosity of 1–4 µm that occurs in darker BSE domains forming an annulus separating T2 and T4. Minor patches with brighter BSE gray tones may represent microinclusions of precursor monazite or new precipitates. The zone T4 are homogenous rims with an uniformly dark BSE gray tone. The rim thicknesses of the T4 rims are greatest where they occur directly adjacent to quenched melt rather than neighboring monazite grains.

Monazite in Upper Greenschist to Amphibolite Facies Meta-Psammopelites

The crystal size of monazite tends to increase with increasing metamorphic grade (e.g., Franz et al., 1996; Rubatto et al., 2001; Wing et al., 2003). In amphibolite-facies meta-psammopelites, monazite grains hardly exceed 150 µm in size and the grain sizes of 30 - 50 µm are common (Schulz, 2017; Schulz et al., 2019b).

Grain shapes display much more variations, contrasting the quite uniform grain shapes of monazite in high-grade rocks and in granites. Short and long prismatic grains with round edges are prevalent (**Figures 4a-c**). Also, amoeboid, lobate and highly irregular grain shapes are abundant (**Figures 4d-g**). Monazite grains with highly irregular shapes may accumulate in distinct layers (**Figure 4h**). Apart from the mostly small grain sizes, monazite in contact metamorphic meta-psammopelites apparently have no discriminant microstructural appearance (**Figures 4i-l**).

There are several detailed reports on monazite mineral chemical compositions from a low pressure terrain with a regional metamorphic zonation in the transition between the Saxothuringian Zone and the Moldanubian Zone in NE Bavaria (Franz et al., 1996; Heinrich et al., 1997). In the adjacent Waldsassen Schiefergebirge a similar geological situation and lithology with staurolite, garnet, fibrolithic sillimanite and cordierite bearing meta-psammopelites has been studied. The Waldsassen Schiefergebirge monazites mostly have overall rectangular shapes and bear many tiny holes and inclusions which sometimes display helicitic planar alignment. The area with oszillatory zonation of the BSE gray tones in the center of the grains follows the general grain shape (**Figures 4m,n**). Textural observations on grain size and shape indicate a continuous growth of monazite from greenschist to granulite facies temperatures in the garnet-poor metapsammopelites (Franz et al., 1996). The minor HREE concentrations and the Y contents in monazite increase strongly with increasing metamorphic grade. Monazite crystals often show zonation with cores low in HREE and Y, and rims high in HREE and Y, that is interpreted as growth zonation attained during prograde metamorphism (Franz et al., 1996; Heinrich et al., 1997).

Specific Microstructures and Their Petrochronological Significance

Zoning in Monazite

In numerous references it is reported that monazite often displays zonation of its chemical composition, however, in many cases the term zonation encloses the patchy and intergrowth-like distribution of areas with different BSE gray tones as described above (e.g., Parrish, 1990; Watt and Harley, 1993; Ayers et al., 1999; Bea and Montero, 1999; Crowley and Ghent, 1999; Hawkins and Bowring, 1999; Williams et al., 1999; Townsend et al., 2000; Pyle et al., 2001; Simmat and Raith, 2008; Brandt et al., 2011). Zhu and O'Nions (1999) distinguished four major types of monazite zoning: (a) Simple concentric zoning; (b) Complex concentric zoning; (c) Intergrowth zoning and (d) Patchy zoning. Border lines between the BSE gray colors of the zonations can be straight, slightly curved, or lobate (**Figures 5a-c**). In granite clasts within the suevite impact breccia from the Nördlinger Ries crater, a Th-rich rim with bright BSE gray color is observed in monazite (**Figure 5d**). This may be common for monazite in granite or a specific impact-related feature. There are examples where the marginal monazite zone encloses numerous needles (**Figure 5e**). Rims are typically higher in Th, though the opposite (low-Th rims) was also observed (**Figure 5f**). Most important are the sharp boundaries between the chemical domains, which suggest that possible post-crystallization diffusional modification of the zoning is below the spatial resolution of the electron microprobe ($\sim$2 μm). In general, Th and U zoning are correlated with Ca, Si, and LREE zoning, consistent with the cation exchange mechanisms. Th and U are often zoned, but their zoning is not always correlated. Pb is correlated with Th and U concentrations and with age. The Y zoning is believed to record a history of monazite growth in many cases (e.g., Heinrich et al., 1997; Pyle et al., 2001). A highly embayed monazite crystal that experiences later growth that fills in the embayments, would have the appearance of an internal core with a composition similar to the rim in a thin section. Interpretations of the growth history of monazite in complexly zoned grains must take into consideration this possibility (e.g., Pyle et al., 2002). It appears also possible that the growth of a monazite grain stopped for any reason and continued later, resulting in a growth hiatus. Such a process may have led to a conchoidal monazite (**Figure 5g**). Age zonations are rare in monazite. In most cases, even significant zonations in BSE gray tones do not correspond to a significant age zonation. The monazite shown in **Figure 5h** is an exception, as the darker part provided Permian and the light rim Cretaceous EPMA Th-U-Pb ages (Schulz, 2017). The growth of significantly younger ($\sim$50 Ma) rims in monazite within garnet biotite sillimanite granulites can be attributed to a fluid-enhanced recrystallization during back-reaction with melt at sub-solidus conditions (Brandt et al., 2011). This interpretation is based on the observation that monazites enclosed in garnet have not such younger rims, as they were shielded against fluid infiltration. Further exceptions (e.g., Pyle et al., 2002; Simmat and Raith, 2008) have important implications with respect to monazite geochronology. The available evidence from such natural monazites with age zonations, including those from the granulite facies, suggests that diffusion has not modified the chemical zoning, including that of Pb, at a scale of > 2 μm. This observation implies that the closure temperature of monazite for Th-U-Pb geochronology exceeds 900°C, consistent with the diffusion study of Cherniak et al. (2004).

Monazite Corona Microstructure

The replacement of monazite by single coronas of allanite and by double coronas with apatite-allanite is often observed (e.g., Broska and Siman, 1998; Finger et al., 1998; Grapes et al., 2005; Upadhyay and Pruseth, 2012). This microstructure is abundant in granites with magmatic monazite that became metamorphosed under greenschist to amphibolite facies conditions. In metapelites, this microstructure has been described when monazite first formed during a metamorphic event at higher temperature and then reacted to apatite plus allanite during an overprint at lower temperatures (e.g., Finger et al., 1998; Wing et al., 2003; Gasser et al., 2012; Skrzypek et al., 2020). The microstructure can also be preserved by static recrystallization when the maximum temperature of a second metamorphic event exceeds those of the first event (Schulz, 2017). The alteration of monazite to allanite and fluorapatite has been experimentally studied by Budzyń et al. (2011). Their work confirms the strong influence of fluid and whole-rock

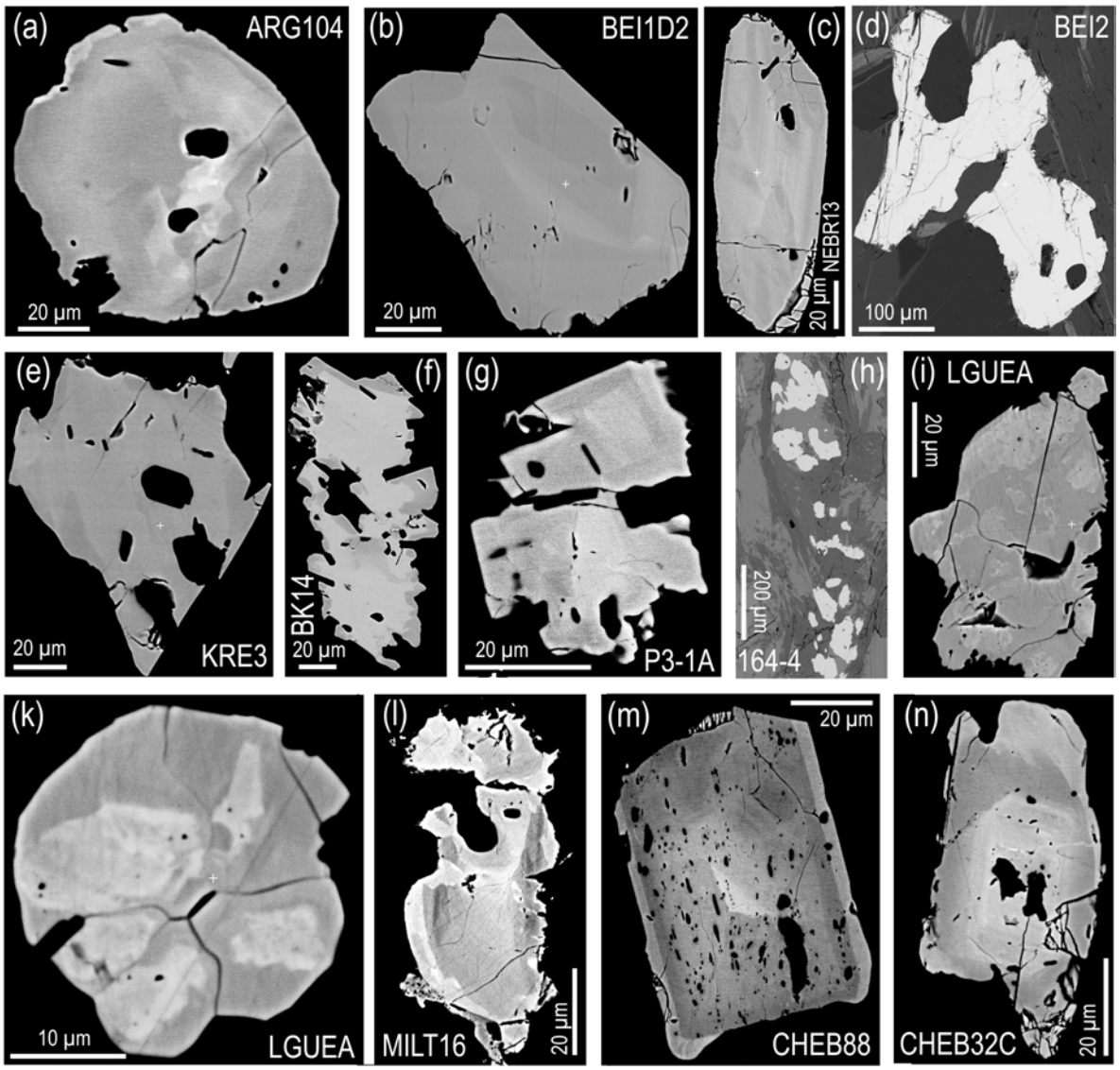

FIGURE 4 | Monazite in amphibolite facies micaschist. **(a)** Euhedral monazite with rounded corners and cloudy Th-rich core zone, Conlara, Argentina (Lopez de Luchi et al., 2020). **(b)** Euhedral and nearly homogeneous monazite with rounded corners in a micaschist from the Cretaceous high-pressure Eclogite Unit of the Saualpe (Schulz, 2017). **(c)** Long prismatic monazite from the Carboniferous amphibolite-facies Austroalpine Oetztal-Stubai Basement, Eastern Alps (Rode et al., 2012). **(d)** Amoeboid grain shape of monazite (Saualpe). **(e)** Irregular grain shape of monazite (Saualpe). **(f)** Highly irregular grain shape of monazite in a micaschist (Central Erzgebirge). **(g)** Highly irregular grain shape of monazite with rectangular and sutured grain boundaries, from "Schiefererz" micaschist, Pöhla, Western Erzgebirge. **(h)** Arrangement of numerous large monazite grains in a quartz-rich layer of garnet micaschist of Moldanubian diaphthorite zone (NE Bavaria). **(i,j)** Contact metamorphic monazite in enclaves of garnet hornfels in the granite of Rostrenen, Central Brittany (Schulz, 2013). **(l)** Monazite in an andalusite micaschist from Miltitz in the Nossen-Wilsdruff Schiefergebirge, Saxothuringian Zone. **(m,n)** Euhedral monazite with zonation and helicitic inclusions in cordierite micaschist from the Waldsassen Schiefergebirge in the Saxothuringian Zone.

composition on the stability of monazite. Both monazite and allanite can occasionally alter to rhabdophane and to REE carbonate minerals like hydroxylbastnaesite-(Ce) or synchysite, when CO_2-rich fluids are present (Ondrejka et al., 2012).

Numerous variations of the corona microstructure are documented in polymetamorphic meta-psammopelites, as in the Carboniferous/Permian amphibolite facies Austroalpine basement units (Rode et al., 2012; Schulz, 2017; Schulz et al., 2019b). A single thin corona defined by decussate or radially oriented prismatic allanite appears as the most elementary structure (**Figure 6a**). A transition to double coronas is given when a thin band of apatite appears between the monazite and the allanite mantle (**Figure 6b**). In this stage, the apatite corona grows by monazite consumption along convex inward migrating grain boundaries (**Figures 6c,d**). There are double coronas where apatite and allanite mantles appear with cloudy BSE gray colors, without a separation into distinct grains (**Figures 6c,g**). This can be seen as the common reaction

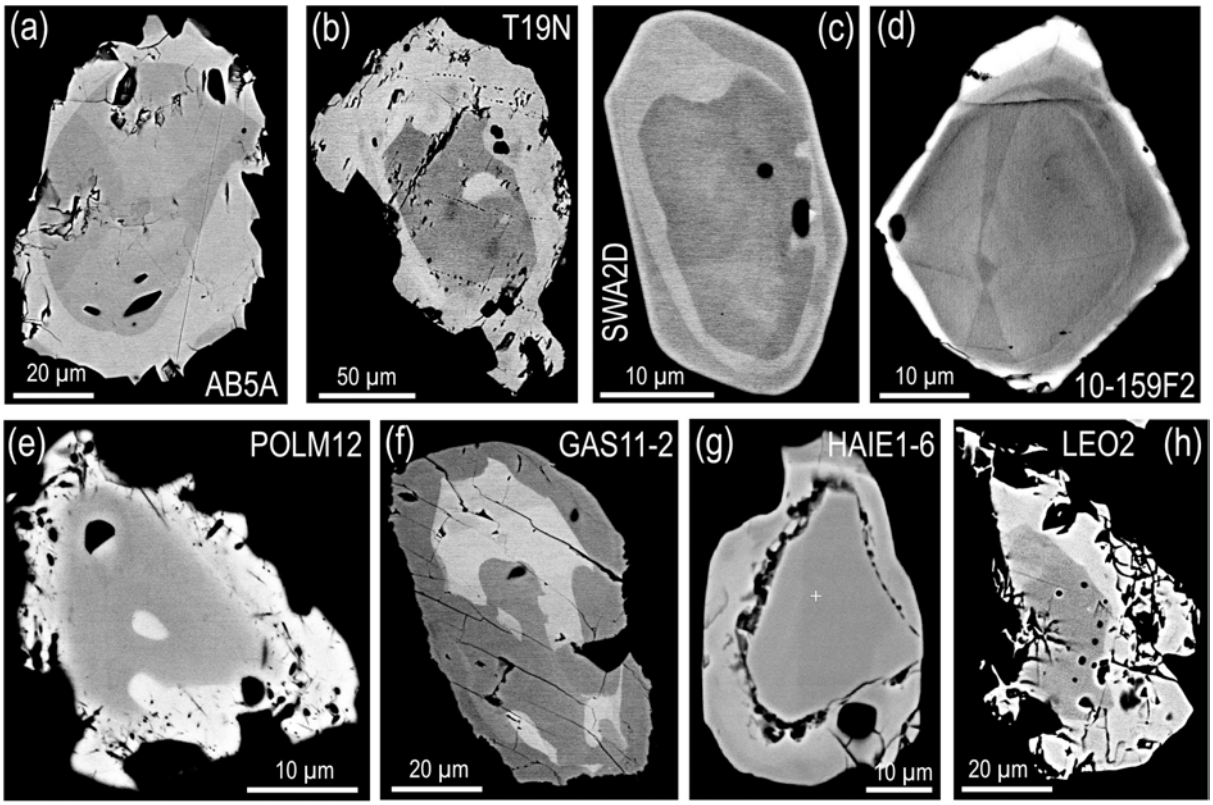

FIGURE 5 | Monazite with striking concentric zonations. **(a,b)** Th-rich broad rim domains in monazites from high-grade gneisses. **(c)** Double concentric zonation of a monazite in high-grade mica gneiss from the Saxonian Granulite Massif. **(d)** Th-rich small rim zone in a monazite from a granite clast in the suevite impact breccia of Nördlinger Ries. **(e)** Monazite with an inclusion- and Th-rich rim zone in the Eibenstock granite, Western Erzgebirge. **(f)** Monazite with Th-poor dark broad rim zone. **(g)** Conchoidal monazite with separated core and mantle in a garnet micaschist from Central Brittany (Schulz, 2013). **(h)** Zoned monazite with dark Permian-age core and bright Cretaceous-age rim in polymetamorphic garnet micaschist from the Saualpe (Schulz, 2017).

structure when monazite is consumed during retrogression. This is in contrast with double coronas, where the apatite and allanite mantles show blocky single grains and the outer mantle contains radially oriented prismatic allanite (**Figures 6h,i**). Such a microstructure may signal a static recovery, annealing, or recrystallization subsequent to the decomposition reactions at constant or increasing temperatures. Different behavior of the Th which was released from decomposing monazite can be observed. The Th can crystallize as tiny thorite within the apatite mantle (**Figures 6d,e**). The tiny thorite grains also can be concentrated at the outer margin of the apatite mantle and inside the allanite corona (**Figure 6f**). The Th may be included in the allanite corona, forming a light halo around the apatite mantle (**Figures 6k,l**). The corona-producing reaction sequence progresses until all monazite is consumed and an inner core by apatite with thorite and a Th-rich inner allanite mantle, and a Th-poor outer allanite mantle remains (**Figures 6k,l**). Also, corona microstructures with apatite core and Th-rich allanite rim are observed (**Figure 6m**). Special variations of the corona structures with inward-directed allanite needles and holes from the removal of water-soluble phosphate phases occur in the Micaschist Unit of the Austroalpine Saualpe basement (**Figure 6n**). Most corona microstructures display a symmetric or concentric configuration. In specific microstructural situations, e.g., when monazite is attached to a garnet, the development of asymmetric corona microstructures can be observed.

Monazite Satellite and Cluster Microstructures

The origin and petrological significance of the monazite satellite structure has been first described by Finger et al. (2016). Their explanations are based on the observation of small monazite grains which straddle around apatite-allanite coronas. The phenomenon has been termed satellite monazites, because the small monazite grains are arranged like satellites concentrically around a core monazite. The combination of satellite monazites and corona structure lead to the hypothesis that the satellite monazites formed through a back-reaction between apatite and allanite. This implicates an important microstructural indicator for a polymetamorphic evolution in meta-psammopelites, especially when the satellite monazites are shown to be significantly younger than the core monazite (Finger et al., 2016). In this case, the satellite grains give evidence of new monazite nucleation and growth (**Figures 7a-d**). Alternatively, when no ages are available, one could argue that the satellites may perhaps just be the undigested remains from the periphery of the primary monazite. In their detailed

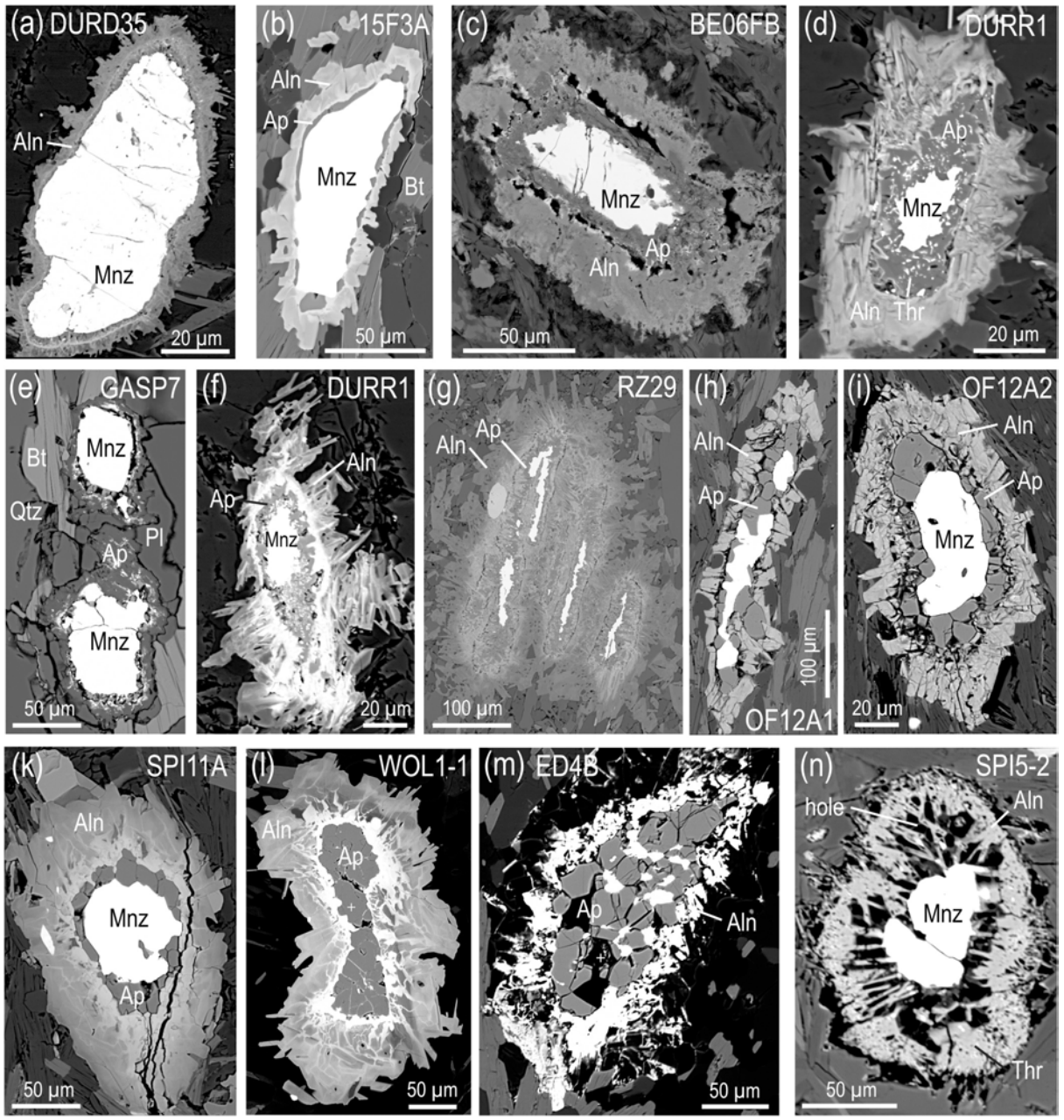

FIGURE 6 | Corona structures of monazite. **(a)** Rim with radial allanite (Aln) crystals mantling a monazite (Mnz), Austroalpine Oetztal-Stubai Basement (Rode et al., 2012). **(b)** Allanite mantle and monazite core are separated by a tiny zone with apatite (Ap). **(c)** Monazite in a phyllite with double corona of inner apatite and outer allanite. **(d)** Monazite core with sutured grain boundary is surrounded by a corona with apatite and tiny thorite (Thr), and a corona with prismatic allanite. **(e)** Monazite cores are surrounded by apatite and thorite. **(f)** Partly consumed monazite with sutured grain boundary is surrounded by apatite and allanite coronas. The inner part of the allanite corona is conspicious by Th-rich allanite. **(g)** Thin relict bands of monazite in apatite-allanite coronas. **(h,i,k)** Corona structures in a Saualpe micaschist. Apatite and allanite grains underwent static recrystallization due to a thermal overprint (Schulz, 2017). **(l)** Corona structure with fully consumed monazite in the apatite core with tiny thorite grains; see light Th-rich inner part of the allanite corona. **(m)** Apatite with corona by Th-rich allanite. **(n)** Allanite crystals with tiny thorite inclusions rim relict monazite in a Saualpe micaschist. The holes may have been water-soluble phospate phases.

description, Finger et al. (2016) reported also about structural modifications of the satellite structure. These are girdles of small satellite monazites around single apatite cores (**Figures 7e,f**). Also, small monazite grains in a satellite arrangement without a distinct core grain (**Figure 7g**) or around fine-grained allanite aggregates (**Figure 7g**) can be considered as variations of the satellite microstructure.

Accumulations of small monazite grains without the distinct satellite arrangement could be labelled as cluster structures. Such clusters can be encountered in various situations. Small monazite

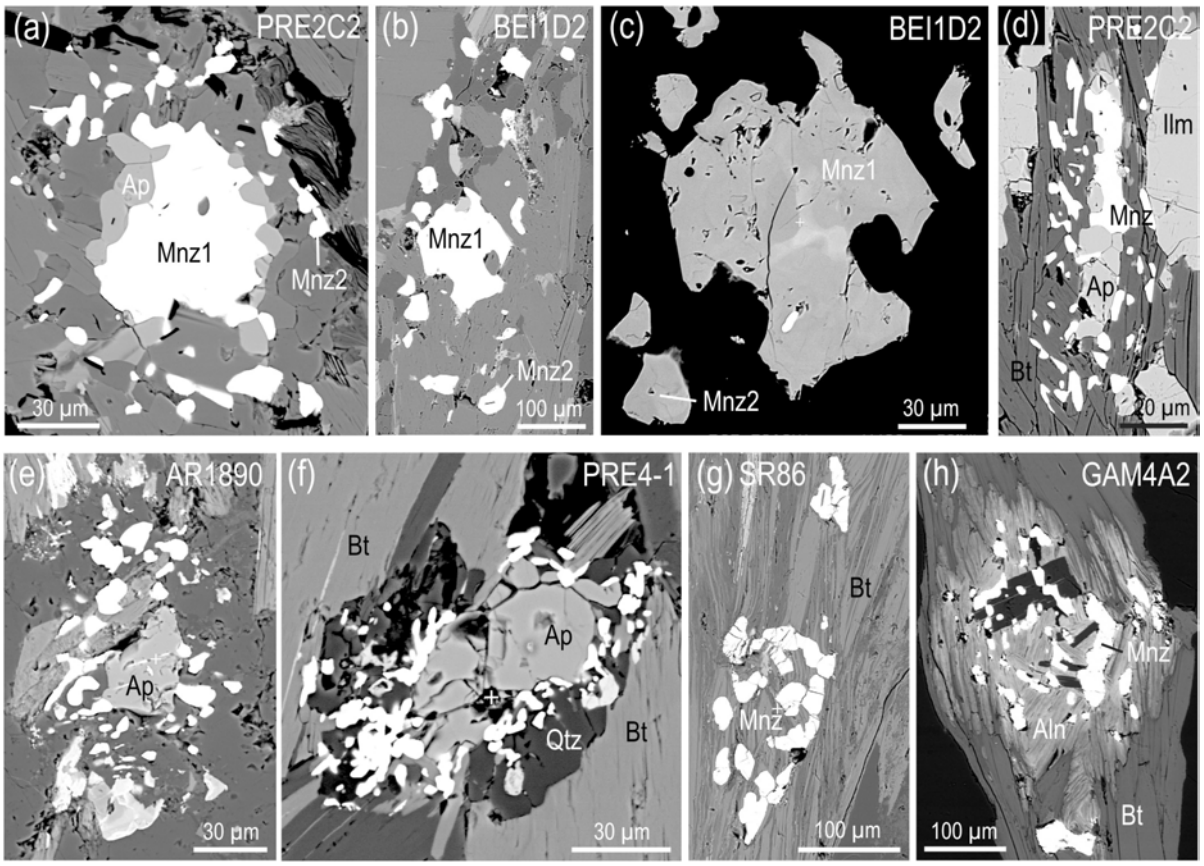

FIGURE 7 | Satellite microstrutures of monazite as defined by Finger et al. (2016). **(a)** Typical satellite microstructure with core monazite (Mnz1) and attached relicts of the apatite (Ap) corona, surrounded by a ring of small monazites (Mnz2) which apparently crystallized from the former allanite corona (Finger et al., 2016). **(b,c)** Elongated satellite structure with amoeboid core monazite in micaschist from the polymetamorphic Saualpe basement (Schulz, 2017). **(d)** Elongated satellite microstructure with apatite and monazite in the core. **(e,f)** Small satellite monazites surrounding an apatite core in micaschists from the Aiguilles Rouges Massif (Schulz and von Raumer, 2011) and from Saualpe. **(g,h)** Arrangements of small monazite grains resembling satellite microstructure.

grains with irregular shapes are observed in the interior of complexly coarse-grained aggregates of allanite (**Figures 8a,b**). Apparently, these small grains are no relics but newly crystallized monazite. In another situation, each monazite grain of the cluster is surrounded by belts of tiny allanite crystals (**Figures 8c,d**) or, is situated in larger aggregates of allanite. When the cluster monazites are markedly younger as the common larger monazite grains in the matrix, this signals that they crystallized at a separate metamorphic thermal or fluid-triggered event. Distinct symplectite aggregates of monazite and allanite are rarely observed in high pressure low temperature micaschists of the Erzgebirge (**Figures 8e-h**). Such structures can be interpreted as a preserved or "frozen" allanite-monazite univariant equilibrium.

Monazite Aggregation Microstructure

The monazite aggregation microstructures contrast the small and isolated grains of the cluster structures. However, it seems that monazite clusters may progressively develop toward aggregates by further nucleation and grain growth. Monazite aggregates were documented in the Saxonian Granulite Massif. In high-grade garnet-free mica gneisses, numerous single monazites with grain sizes of 10 - 15 µm form polygonal aggregates of up to 200 µm length (**Figures 9f,b**). Straight monazite grain boundaries which meet at angles of 120° resemble static recrystallization. Such aggregates could represent an initial stage of the formation of large monazites in high-grade rocks. There is yet no data on the crystallographic orientation of the single small monazite grains and the crystallographic development during their aggregation.

Another sort of monazite aggregation appears in granite and micaschist which underwent an overprint at upper greenschist facies conditions. In the sheared Erinpura granite (**Figure 9c**), an initial stage is observed by the formation of small isolated monazite grains with irregular shape in biotite-rich parts (Just et al., 2010). In the next stage, observed in micaschist, numerous large (∼50 µm) and small (<10 µm) individual monazite grains agglomerate to form grains with strongly sutured grain boundaries and irregular shapes (**Figures 9d,e**). The progressive coalescence of the individual grains with many tiny inclusions and also small thorite leads to larger grains with a patchy sipped internal distribution of BSE gray tones (**Figures 9f,g**). These aggregated monazites have grain sizes of up to 50 µm. A special

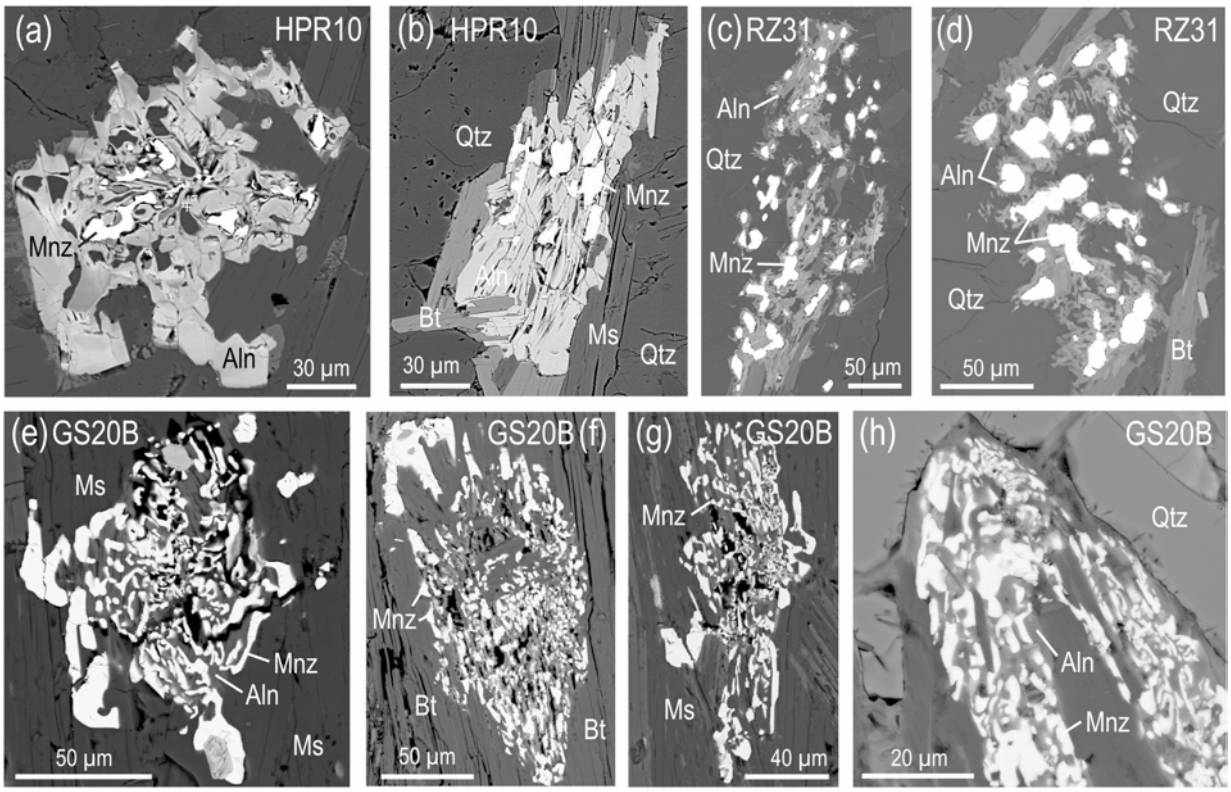

FIGURE 8 | Monazite cluster and symplectite structures. **(a,b)** Small Cretaceous monazite grains (Mnz) in a polycrystalline aggregate of allanite (Aln) in a micaschist from the Austroalpine Schobergruppe (Krenn et al., 2012). **(c,d)** Clusters of small monazite grains with mantles of allanite in micaschist from the Oetztal-Stubai Basement (Schulz et al., 2019b). **(e-h)** Symplectites of monazite and allanite in high pressure low temperature micaschist from the Western Erzgebirge.

sort of aggregate are coatings by monazite around other minerals. Monazite coats around detrital zircon have been described from migmatised paragneisses (Aleinikoff et al., 2012a). Monazite coating of ore minerals may give age indications of hydrothermal processes (Aleinikoff et al., 2012b). A coating aggregate was found in garnet micaschists of the lower tectonic unit in the Münchberg Nappe in the Saxothuringian Zone of the Variscides (Schulz et al., 2017). Narrow-spaced rounded small apatite grains of 10 - 20 µm size which are all coated by monazite (**Figure 9h**). Together with adjacent monazite grains, this results in net-like aggregates of up to 200 µm length. Like the other types of aggregates, this structure can be interpreted to have formed by monazite nucleation and growth.

Sponge-Like Microstructures of Monazite Decomposition

Observations at high BSE contrast in monazite in granites and in meta-psammopelites revealed internal fine-meshed structures, referred here as sponge-like microstructures (**Figure 10**). As these microstructures are occasionally observed in rocks which underwent hydrothermal overprint or retrogression (e.g., Read et al., 2002), they are interpreted as a sort of reaction structure with an intra-grain decomposition of monazite. Monazite can be completely replaced by pseudomorphs of allanite. This is supported by the appearance of small thorite in the center of the grains (**Figures 10a,b**). Often the sponge-like structures encompass only the marginal parts of the monazite grains and the internal parts remain unaffected. In marginal parts with darker BSE gray color where the monazite sponge-like structure disappears, apatite is observed (**Figure 10e**). As apatite can accommodate only small proportions of the Th from the decomposing monazite, the remaining Th is consumed by crystallization of small thorite grains within the apatite. It is also observed that the sponge-like monazite recrystallizes *in situ* as pseudomorphs, with thorite, fibrolithic rhabdophane, bastnaesite, britholite, or other REE-bearing minerals (**Figures 10f-h**).

Inclusions of Monazite

Inclusions of monazite in host minerals apart from apatite, allanite and epidote provide interesting insight to the crystallization-deformation sequence of a rock. Mostly, monazite is enclosed in biotite, even when large grain sizes are realized (**Figure 11a**). It appears that biotite is a preferred microstructural domain for metamorphic monazite crystallization (e.g., Schulz et al., 2019b). Monazite can be enclosed by Fe-Ti minerals as ilmenite or as well in staurolite (**Figures 11b,c**). When monazite is enclosed by quartz or feldspar it appears as protected and less vulnerable for fluid-induced dissolution-reprecipitation or decomposition, and may

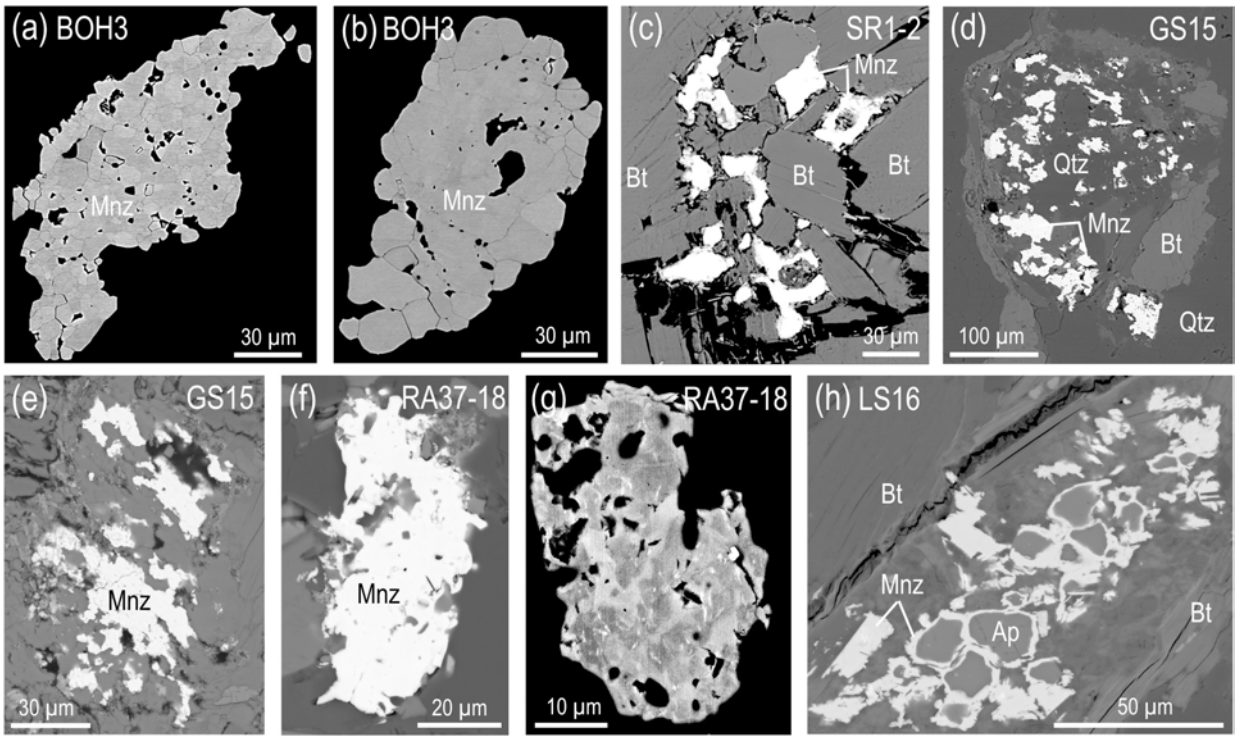

FIGURE 9 | Monazite crystallization and aggregation microstructures. **(a,b)** Large polycrystalline aggregates composed of numerous small monazite (Mnz) with static grain boundaries in high-grade mica gneiss from the Saxonian Granulite Massif. **(c)** Nucleation of small monazite in a biotite-rich domain (Bt) in a sheared Erinpura granitoid (Just et al., 2010). **(d)** Cluster-like assemblage of monazite grains with highly sutured and irregular grain boundaries, with quartz (Qtz) and biotite (Bt). **(e)** Larger monazites with highly sutured and irregular grain boundaries aggregated with surrounding smaller grains. **(f,g)** Aggregated monazite grains. The aggregated character can be recognized by irregular and sutured grain boundaries, the clumped small domains with different Th contents, and the numerous small inclusions (Oriolo et al., 2019). **(h)** Monazite rimming apatite (Ap) grains and forming a net-like aggregation in a micaschist from the Lower Unit in the Münchberg Nappe, Saxothuringian Zone.

thus better conserve its Th-U-Pb information (**Figure 11d**). Of special interest for petrochronology are small monazite inclusions in garnet, as claimed in numerous studies (e.g., Pyle et al., 2001; Pyle et al., 2002; Berger et al., 2005). Potentially, the monazite inclusions in garnet allow to link the P-T path record by the garnet Ca-Mg-Mn-Fe zonations in limited mineral assemblages with biotite, muscovite, plagioclase, aluminosilicates, sometimes cordierite, and quartz to the age of monazite. A general and preliminary assumption is, that monazite should be older than the hosting garnet. However, this is highly questionable, as a metamorphic garnet crystal is usually pervaded by tension cracks which may have given access to fluids for an intragranular post-garnet monazite growth (**Figures 11e-h**). Garnet may postdate its monazite inclusions when these are markedly older than the bulk of the matrix monazites. Garnet can enclose monazite in the internal structures of a syntectonic growth or a syncrystalline rotation (**Figure 11i**), the helicitic or snowball structures as detailed in Passchier and Trouw (2005). It has been demonstrated by the analysis of Y in enclosed monazite and in garnet, that monazite crystallized at the same time or after the hosting garnet (Schulz, 2014). In this case, the ages of monazite enclosed and in the matrix are similar.

INTERPRETATION OF MONAZITE MICROSTRUCTURES IN PETROCHRONOLOGY

It has been recognized in very early accessory mineral studies (e.g., Lee and Dodge, 1964; Lee and Bastron, 1967) that monazite and allanite are not stable together. Monazite can react to allanite plus apatite and vice versa (e.g., Finger et al., 1998; Wing et al., 2003). Whether monazite or allanite occurs in a metamorphic rock is determined by whole-rock composition and the metamorphic grade (Janots et al., 2007, 2008; Spear, 2010). Accordingly, monazite is stable in metapelites under amphibolite facies conditions. The monazite stability field is shifted toward lower temperature with decreasing bulk rock Ca (**Figure 12**). Also, the stability field of monazite is extended to lower temperature with increasing Al. As a consequence, monazite can be expected to crystallize at upper greenschist facies conditions in high-Al and low-Ca metapelites (e.g., Spear, 2010; Spear and Pyle, 2010). A higher Ca whole-rock content expands the allanite stability field to higher temperatures and the monazite stability field then retreats to granulite facies conditions (Bingen et al., 1996). The extend of the monazite stability field at a pressure above ∼14 kbar is poorly constrained

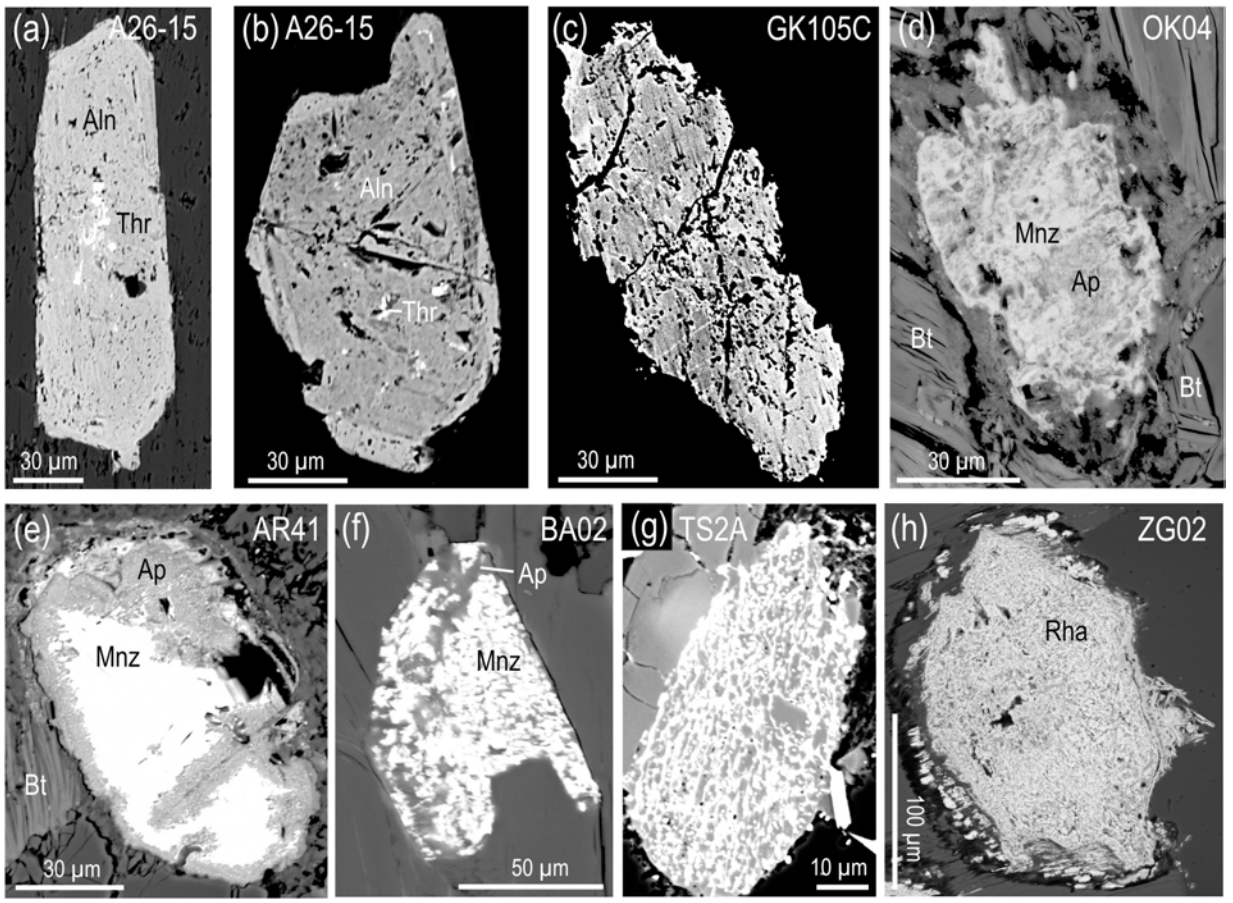

FIGURE 10 | Sponge-like microstructures of monazite decomposition and decay. **(a,b)** Allanite (Aln) pseudomorph of former monazite with numerous thorite (Thr), and anhedral monazite with numerous tiny holes and thorite inclusions in a zone of hydrothermal overprint, Bushmanland Terrane, Namaqua Province, RSA. **(c)** Internally corroded monazite with numerous elongated holes. **(d)** Relict monazite sponge microstructure with apatite (Ap) in micaschist from the Lower Unit in the Münchberg Nappe, Saxothuringian Zone. **(e)** Partial and graded decomposition of monazite to apatite in a micaschist from the Aiguilles Rouges Massif (Schulz and von Raumer, 2011). **(f,g)** Sponge-like intergrowth of monazite relicts and apatite pseudomorphing a large monazite grain. **(h)** Complete transformation of a large monazite grain to a pseudomorph of fibrolithic rhabdophane (Rha) in Zinnwald greisen granite.

by experiments and thermodynamic modelling (Spear, 2010). However, the isopleths of the Ca bulk rock composition limiting the monazite stability field are mainly temperature-dependent but also inclined with increasing pressure (**Figure 12**).

Garnet-bearing meta-psammopelites allow at least a partial reconstruction of the pressure-temperature evolution by equilibrium thermodynamic methods, such as geothermobarometry by cation exchange and net transfer continuous reactions, or alternatively, by pseudosection modelling (Powell and Holland, 1994, 2008; Holland and Powell, 1998, 2011). In numerous cases, the garnet-bearing assemblages recorded a prograde metamorphism with increasing pressure (P) and temperature (T), followed by decrease of P at further increasing T. The maximum temperatures are reached during the decompression. This represents the standard clockwise P-T path in a continental collision scenario with tectonic crustal thickening, as outlined in the numerical models by England and Thompson (1984) and Thompson and England (1984). The rates of the decompression-heating toward Tmax and the rates of the subsequent decompression-cooling are controlled by a plurality of tectonic and magmatic processes. Reports on counterclockwise (or anticlockwise) P-T paths are comparably rare. Pyle and Spear (2003) described counterclockwise P-T paths from migmatites in SW New Hampshire which started at low pressure of around 4 kbar and reached a P-Tmax, which allowed partial anatexis with generation of granitic melts. As outlined in numerous detailed studies, correlation of mineral chemical compositions and ages of monazite provides an unique way to understand the development of the microstructures. Crystallization of monazite in rocks which allow an independent reconstruction of their P-T evolution opens one more option to relate the microstructures to geodynamic processes.

As monazite is an accessory mineral in peraluminous granites, the so-called S-type granites (Barbarin, 1998), the decompressional melting along path A, as well the low-pressure melting path B should be considered for interpretation of its microstructures (**Figure 12A**). In the case of the clockwise path A, the first melting could occur at around 650°C, when the XH_2O

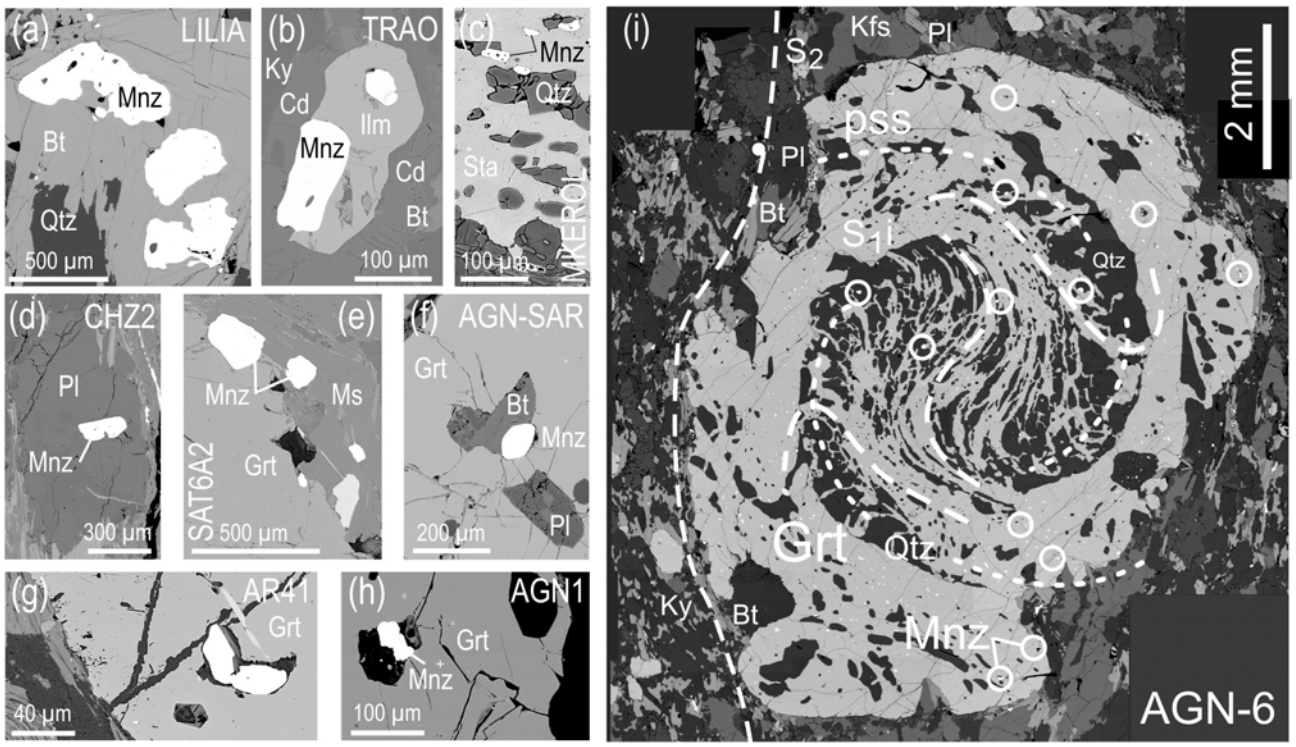

FIGURE 11 | Monazite as inclusions in other minerals. **(a)** Huge anhedral monazite enclosed in biotite in a migmatite from Lilia, Léon Domain (Schulz et al., 2007). **(b)** Inclusion in ilmenite (Ilm) in a cordierite (Cd) garnet gneiss, Léon Domain. **(c)** Inclusion in staurolite in micaschist from Central Brittany (Schulz, 2013). **(d)** Inclusion in plagioclase in garnet gneiss from the Lower Gneiss Unit, Haut Allier, French Massif Central (Schulz, 2014). **(e)** Garnet in a UHP gneiss from Central Erzgebirge partly encloses monazite of Carboniferous age in its rim. **(f)** Monazite with biotite in garnet in a kyanite garnet gneiss from the Upper Gneiss Unit, French Massif Central. **(g,h)** Cracks in the garnet connect monazite inclusions with the matrix. **(i)** Example of a syntectonic helicitic garnet with S-shaped internal foliation (S1i) and double pressure shadow inclusion spiral (pss) enclosing numerous monazites (marked by rings). Detailed analysis of yttrium contents in monazite and garnet suggest that the Carboniferous monazites crystallized at the same time or later as the garnet (Schulz, 2014).

is at 1.0, or at higher temperatures, for lower XH_2O (**Figure 12A**). As the pre-melting path A is mostly outside the monazite stability field, no significant crystallization of pre-granitic monazite can be expected. When the granitic melt crystallizes after an adiabatic ascent, formation of monazite can be expected, preferably in Ca-poor and Al-rich granitoid compositions (**Figure 12A**). The expected microstructural evolution along the counterclockwise melting path B considerably differs from path A. There, the melting path B is almost entirely in the monazite stability field and passes dehydration reactions (**Figure 12A**). The fluids released from muscovite (and later biotite) decomposition may enhance crystallization and precipitation of monazite until melting conditions are achieved. It may appear that pre-melt monazite or parts of it remain in the melt as an inherited accessory phase (Yakymchuk, 2017). Also, when the granitic melt crystallizes after adiabatic ascent, it will reach low pressures, which are again favorable for monazite formation. As a consequence, one could expect a considerably higher potential for monazite formation and microstructure development in the case of path B, as it has been outlined by Pyle and Spear (2003).

Clockwise P-T paths have been reported from aluminous garnet-bearing gneisses ("kinzigites") and granulite gneisses (**Figure 12B**). In the case of aluminous and Ca-poor bulk rock compositions, the entire prograde and retrograde evolution occurs within the monazite stability field. However, for Ca-richer compositions, it appears that the monazite stability field is achieved at decreasing pressure when maximum temperatures are approached. Then, monazite crystals will nucleate and grow. Correspondingly, one can expect monazite cluster and aggregation microstructures, and in the case of polymetamorphism, satellite microstructures. When temperatures further increase, as in the case of high temperature metamorphism, these initial stages of monazite nucleation and growth will be succeeded by formation of large monazite grains. As a consequence, the Th-U-Pb system of the monazite will indicate an age of a post-Pmax evolution. Also the post-Tmax evolution along such a clockwise P-T path will continue within the monazite stability field until the univariant line of an allanite-producing reaction is passed. Dependent on the bulk rock Ca-Al composition and the availability of reaction-enhancing fluids, one can expect monazite decomposition with sponge-like or corona microstructures. In such a scenario, the monazite ages are expected to cover the time span of the P-T evolution within the monazite stability field. In the histogram pattern of the monazite Th-U-Pb ages, a maximum of data may give the time of Tmax or even post-Tmax, depending on the cooling rates.

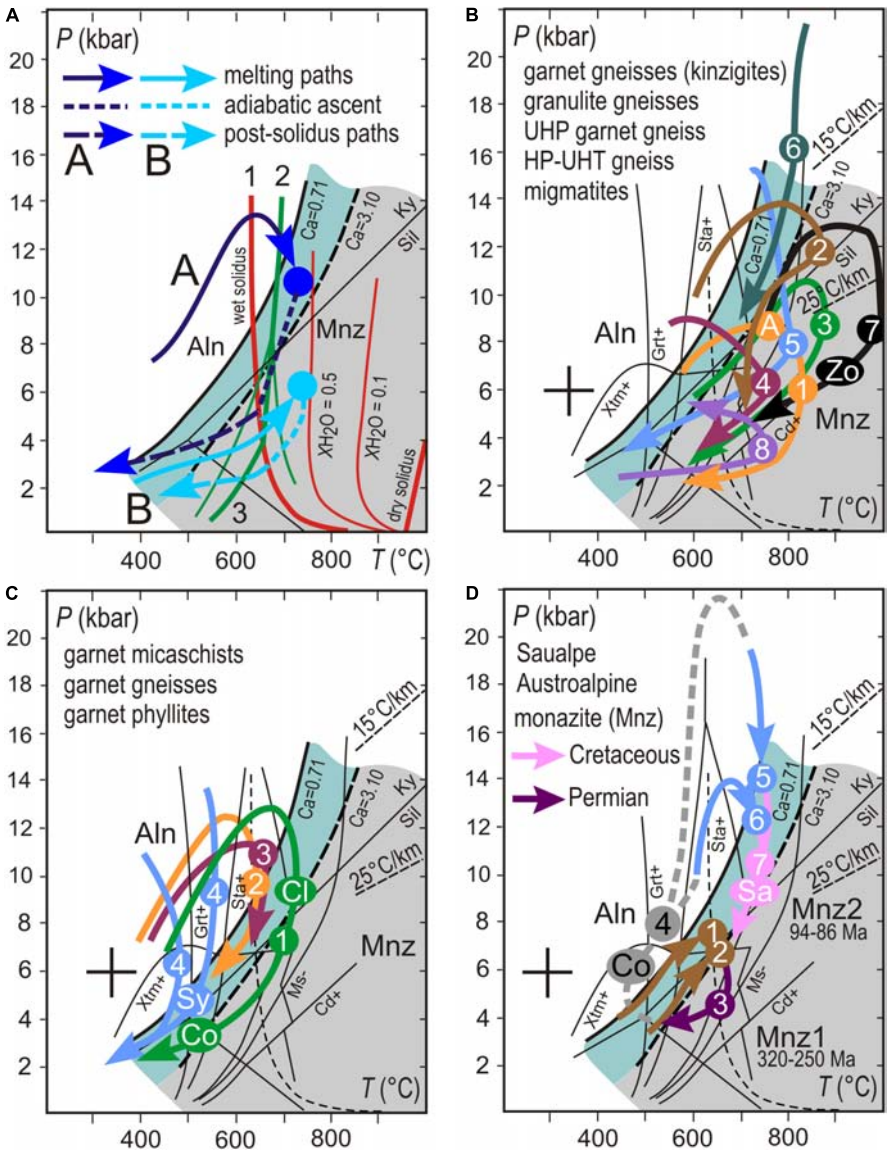

FIGURE 12 | Pressure-temperature evolution of monazite-bearing granites and P-T path reconstructions from metamorphic rocks. Characteristic monazite microstructures are indicated with abbreviations. Stability fields of monazite (Mnz) and allanite (Aln) at different bulk rock contents as a function of Ca wt%, and with the xenotime (Xtm) stability field after Janots et al. (2007) and Spear (2010). Petrogenetic grid for metapelites in the KFMASH system with major reactions in black lines are compiled from Spear (1993). Cross marks a general uncertainty of ± 50°C/1.0 kbar on geothermobarometric estimates. Red lines are solidus curves in the granitic system Qtz-Ab-Or-H_2O at XH_2O of 1.0 (curve 1), at XH_20 of 0.5 and 0.1 after Johannes and Holtz (1996). Green lines display the reaction Ms + Qtz + Pl = Ky + Kfs + melt (curve 2) and the muscovite-out reaction Ms + Qtz = Sill + Kfs + H_2O at XH_2O of 1.0 (curve 3) and at XH_2O of 0.5 after Kerrick (1972). **(A)** Partial anatexis of crustal rocks (colored dots) by decompressional melting (path A) and low pressure melting (path B). Granitic melts underwent adiabatic ascent and crystallization. Melting path and post-solidus path A is mostly outside and at the margin of the monazite stability field. Major part of melting path and post-solidus path B is in the monazite stability field. **(B)** P-T paths of high-grade metamorphic rocks. 1 - cordierite garnet gneisses, Saxonian Granulite Massif (Schulz and Krause, 2018), with aggregation microstructure (A). 2 - kyanite garnet gneiss, Upper Gneiss Unit, French Massif Central (Schulz, 2014). 3 - cordierite garnet gneiss, Herbon Farm, Golfe de Morbihan, Southern Brittany (Schulz, 2013). 4 - hercynite cordierite garnet gneiss, Moldanubian Zone (Schulz, 2010). 5 - garnet gneisses, Léon Domain, Northern Brittany (Schulz et al., 2007). 6 - UHP garnet gneiss, Central Erzgebirge (Massonne, 2003). 7 - HP-UHT garnet biotite sillimanite granulite from Palni Hills, South India (Brandt et al., 2011), with monazite age and compositional zonation (Zo). 8 - counterclockwise P-T evolution in migmatites, SW New Hampshire (Pyle and Spear, 2003). **(C)** P-T paths of upper greenschist to amphibolite facies rocks with monazite and garnet. 1 - Oetztal-Stubai Basement (Schulz et al., 2019b), with cluster (Cl) and corona structures (Co). 2 - Lower Unit, Münchberg Nappe, Saxothuringian Zone (Schulz et al., 2017). 3 - North Patagonian Basement in Argentina (Oriolo et al., 2019). 4 - Phyllite and micaschist units of the Western Erzgebirge (Mingram and Rötzler, 1999; Willner et al., 2000), with symplectite structure (Sy). **(D)** Case study of monazite crystallization and decomposition during polyphase metamorphism of Austroalpine Saualpe basement (Schulz, 2017). 1, 2 - garnet 1 crystallization in the Eclogite and Preims nappe units. 3 - Permian monazite 1 (Mnz1) crystallized during intrusion of numerous pegmatites. 4 - inferred retrogressive and compression path between garnet 1 and garnet 2 crystallization, with corona structures (Co) around Permian monazites. 5, 6 - garnet 2 crystallization in the Eclogite and Preims nappe units. 7 - Cretaceous monazite 2 (Mnz2) crystallization during decompression, partly in satellite structures (Sa).

This age distribution may provide also insights into the rates of metamorphic processes taking place within the monazite stability field. As already stated above, monazite crystallization is favored along the low pressure prograde part of counterclockwise P-T paths. Pyle and Spear (2003) reported such a scenario from migmatites (**Figure 12B**). During a prograde evolution, several fluid-producing reactions as well as melt-producing univariant reaction lines are passed. A complex sequence of monazite growth and consumption has been derived from the observation of four monazite generations, where three of them are apparently linked to specific whole-rock reactions (Pyle and Spear, 2003).

According to numerous case studies, the clockwise prograde P-T evolution of upper greenschist to upper amphibolite facies meta-psammopelites, occurs in large parts outside the monazite stability field, even for high-Al and low-Ca bulk compositions (**Figure 12C**). At best, the monazite stability field will be entered at Tmax and during a later stage of decompression. Studies in amphibolite facies metapelites have identified a major pulse of monazite growth, which could be linked to the breakdown of garnet at decreasing pressure (Pyle et al., 2001; Spear, 2010). Due to the position of the monazite-allanite reaction isopleths, monazite will crystallize along the decompression-cooling path. The expected monazite microstructures are clusters and aggregations. Such microstructures will be potentially preserved and not overwhelmed by subsequent crystallization of large monazite grains, as the maximum temperatures were already achieved. In the special case of the monazite-allanite symplectite microstructures (**Figures 8e-h**), the decompression-cooling path may have reached and followed the P-T trace of the univariant monazite-allanite reaction at the given bulk composition.

It is important to consider that meta-psammopelites may undergo progressive shearing and deformation during their burial and heating, but also during the cooling, uplift and exhumation. This leads to the presence of high strain domains or foliations surrounding low strain domains with a different mineralogy, and, thus bulk composition. As a consequence, the Al-Ca contents can vary considerably among the microstructural domains, favoring or restraining the monazite crystallization. In addition, localized deformation in high-strain domains may catalize specific reactions that may not occur in low-strain domains, which may in turn record a metastable mineral assemblage. Dependent on rates and the regional tectonic situation, the decompression-cooling stage is characterized by entrance of fluids in combination to formation of shear zones. Both can enhance the crystallization of monazite in cluster and aggregation microstructures. This offers the opportunity for the dating of such events also by Th-U-Pb analysis of the small monazite grains (e.g., Tchato et al., 2009; Just et al., 2010; Williams et al., 2017; Oriolo et al., 2018, 2019).

Zoned garnet in a meta-psammopelitic mineral assemblage will allow P-T estimates and the reconstruction of distinct parts of the P-T evolution. Even when homogenized or modified by diffusion at high temperatures near to and above ∼800°C, the peak temperature and a part of the retrograde evolution may be extracted (e.g., Spear, 1993; Brandt et al., 2011). The question is then, to which stage of the garnet crystallization, pre-, syn- or post-garnet, monazite ages do correspond. As outlined in Pyle et al. (2001), the Y content of monazite could provide an indication. Garnet and monazite are both the main sinks of the bulk rock Y fractionation. Thus, a pre-garnet grown matrix monazite should have elevated Y contents. However, Y-poor monazites are often observed in garnet-rich high-grade meta-psammopelites (Schulz et al., 2007; Schulz, 2014; Schulz and Krause, 2018). This does not indicate low crystallization temperatures of monazite, as may be inferred from Y-in-monazite thermometry (Heinrich et al., 1997; Pyle et al., 2001). It seems likely that Y is bound in the abundant garnet, so that monazite remains undersaturated in Y. This implicates a post-garnet growth of monazite. It is also interesting to compare the Y contents and ages of monazite from garnet-bearing kinzigites and related gneisses with no garnet. Monazites in gneisses without garnet display low- to high Y contents and an age span of 358 to 355 Ma, whereas the Y-poor monazites from cordierite garnet gneisses display an age span of 340 - 317 Ma (Schulz and Krause, 2018). This would allow the interpretation that monazite crystallization may be prevented during garnet growth, so that monazite in a garnet-free rock grew comparably early and thus recorded an earlier stage of the metamorphic evolution.

Monazite has proven its great potential to record the chronology of polymetamorphism and also of successive events along a single metamorphic circle in many case studies (e.g., Finger et al., 2002; Foster et al., 2004; Finger and Krenn, 2007; Simmat and Raith, 2008; Thöny et al., 2008; Krenn et al., 2009, 2012; Schulz and von Raumer, 2011; Wawrzenitz et al., 2012; Imayama and Suzuki, 2013; Mottrama et al., 2014; Williams et al., 2017). Finger et al. (2016) have claimed that the monazite satellite microstructure gives evidence of a distinct second crystallization event along increasing temperatures, subsequent to a retrogression with the formation of the corona microstructure. These monazite microstructures have been evaluated in the Saualpe in Carinthia (Austria), which is known for its polymetamorphic evolution (Frey et al., 1999; Thöni, 1999; Thöni et al., 2008). Two generations of garnet and monazite are observed (Schulz, 2017; Schulz and Krause, 2021). Geothermobarometry of garnet 1 assemblages signals a crystallization along an M1 prograde metamorphism (**Figure 12D**). Pervasive Permian high-Y and high-Gd monazite 1 formation coincided with the widespread intrusion of Permian pegmatites (**Figure 12D**). Corona microstructures around the large Permian monazites signal a retrogressive stage (**Figures 6h-l,n**). Also, the garnet 1 porphyroblasts display deeply embayed resorption zones. These microstructures suggest that the prograde M1 event had a Permian minimum age and was followed by a retrogression event. The M2 event with garnet 2 postdates the corona formation around Permian monazites, as corona microstructures are enclosed in garnet 2. Garnet 2 records a second prograde P-T evolution, which passed through high pressure conditions. A monazite 2 population with ages from 94 - 86 Ma and with lower Y and Gd contents crystallized at decreasing pressure when the P-T path entered again the monazite stability field (**Figure 12D**). The monazite 2 crystallized in satellite microstructures (**Figures 7a-d,f**) but also in large grains (**Figures 4b,d,e**). Accordingly, the garnet

2 as well as the monazite 2 belong to the Cretaceous high pressure metamorphism M2 (Schulz, 2017; Schulz and Krause, 2021). Apart from the garnet 1 resorption rims, a critical indication that the garnet 1 and 2 generations with both prograde zonations are related to separate P-T cycles and do not record distinct P-T segments along a single P-T cycle comes from the monazite corona microstructures. They give additional evidence of a significant retrogressive stage in between the garnet crystallization events.

CONCLUSION

Monazite is an accessory phase in peraluminous granites, syenite and granitic pegmatites, quartz veins, and carbonatites. It is also a common accessory mineral in metapelitic rocks with Ca-poor and Al-rich bulk compositions at all metamorphic grades above the upper greenschist facies. It has variable mineral chemical compositions which are partly controlled by the monazite - xenotime exchange Y = REE. Also, the huttonite exchange Th + Si = REE + P, and the cheralite Th + Ca = 2REE exchange can operate. Common Pb is negligible when compared to radiogenic Pb resulting from the decay of Th and U, diffusion rates for radiogenic Pb are extremely low at high temperatures, and radiation damage is very limited by self-annealing. Therefore, bulk Th, U, and Pb concentrations in monazite allow for the calculation of ages even from small grains (>10 μm), in addition to isotopic *in situ* dating methods. Grain sizes of most igneous and metamorphic monazite in petrographic thin sections range below 200 μm, and are mostly 100 - 10 μm. Electron-beam based analytical instruments as scanning electron microscope and electron probe microanalyzer with detectors for imaging and element mapping are essential for the documentation and analysis of monazite.

An emanating number of detailed field and experimental studies document microstructures of monazite from different geodynamic and tectonic settings under variable physico-chemical conditions. Monazite microstructures may be sorted in terms dissolution-reprecipitation with primary and secondary crystallization, enclosing nucleation, growth, aggregation and annealing, and decomposition via apatite- and allanite-producing reactions under retrogression and temperature decrease. Monazite microstructures also vary depending on the host rocks (peraluminous granitoids, high-grade metamorphic to granulite facies gneisses, and upper greenschist to amphibolite facies meta-psammopelites). Monazite grains in these host rocks range from euhedral to anhedral, from elliptical over amoeboid to strongly emarginated shapes. Internal structures of the grains enclose oscillatory zonation in some igneous monazite. Single to complex concentric zonations as well as turbulent and cloudy internal structures at low to high BSE gray color contrasts are observed. Comparison to results of experiments with alkali-bearing fluids allow to identify internal microstructures of fluid-mediated dissolution and reprecipitation as convex inward curved Th poor and Th-rich zones and colloidal zonations in monazite in migmatites and overprinted granulite facies host rocks.

Specific monazite microstructures are particularly relevant for petrochronological studies. The monazite corona structure with the partial to complete replacement of monazite by apatite and allanite is interpreted to signal a retrogression event. In contrast, the satellite and cluster microstructures are interpreted to indicate a new monazite nucleation and growth. When the small satellite monazite grains which surround a core monazite are significantly younger as the core and large matrix monazite grains, this implicates a polymetamorphic evolution with retrogression followed by re-heating. Monazite aggregation microstructures are considered to document further grain growth after initial nucleation, whereas polygonal aggregates appear as the initial stage of the formation of large monazites in high-grade rocks. Sponge-like microstructures are interpreted to indicate monazite decomposition. It is also observed that the sponge-like monazite recrystallizes *in situ* as pseudomorphs, with thorite, fibrolithic rhabdophane, bastnaesite, britholite or other REE-bearing minerals.

Garnet-bearing meta-psammopelites allow at least a partial reconstruction of their pressure-temperature evolution by equilibrium thermodynamic methods. An examination of the P-T paths and their relation to the monazite P-T stability field is critical for the understanding of monazite microstructures and the dating of metamorphism. In addition, the garnet-bearing rocks are particularly relevant for monazite petrochronology due to Y fractionation in garnet and monazite, which also provides some hints on their relative timing of crystallization. Igneous monazite crystallization in peraluminous granitic melts may be controlled by P-T paths leading to decompression melting or, alternatively, to low-pressure melting. For some high-grade rocks which underwent clockwise P-T paths, it can be shown that the entire prograde and retrograde P-T evolution occurs within the monazite stability field. Also, monazite crystallization is favored along the low pressure prograde part of counterclockwise P-T paths and may result in a complex sequence of monazite growth and consumption. In contrast, for many upper greenschist to amphibolite facies and also high pressure meta-psammopelites, the monazite stability field is entered at decreasing pressure. Monazite crystallization may then appear at the retrograde stages of the evolution, which would be suitable for monazite dating of late shear zone formation. The corona and satellite microstructures support the potential of monazite dating of complex and polyphase metamorphism.

Monazite microstructures provide an unique potential for the understanding and reconstruction of tectonic scenarios and geodynamics. This is given by monazite mineral chemistry and age dating which allow deep insight to the microstructure formation and development. The common occurrence of monazite in garnet-bearing meta-psammopelites then allows additional and independent constraints of the P-T-time evolution.

AUTHOR CONTRIBUTIONS

The author confirms being the sole contributor of this work and has approved it for publication.

FUNDING

The Deutsche Forschungsgemeinschaft DFG supported numerous field studies on monazite Th-U-Pb dating by grants (SCHU-676/10, 676-11, 676-12, 676-13, 676-15, and 676-20). The Open Access and APC was financed by the Publication Fund of the TU Bergakademie Freiberg.

ACKNOWLEDGMENTS

The author appreciates the initiation and permanent motivation for monazite studies through Fritz Finger from Salzburg. Electron-microprobe monazite dating required long-term analytical sessions which were facilitated at Geozentrum Nordbayern of Universität Erlangen-Nürnberg, Institute of Materials Sciences at TU Bergakademie Freiberg/Saxony and with Joachim Krause at Helmholtz Institute Freiberg for Resource Technology. Support at the SEM studies in the Laboratory of Geometallurgy at TU Bergakademie Freiberg was accomplished by Sabine Gilbricht. Several reviewers contributed with constructive comments to the manuscript and Sebastián Oriolo provided valuable editorial support.

SUPPLEMENTARY MATERIAL

The Supplementary Material for this article can be found online at: https://www.frontiersin.org/articles/10.3389/feart.2021.668566/full#supplementary-material

REFERENCES

Aleinikoff, J. N., Grauch, R. I., Mazdab, F. K., Kwak, L., Fanning, C. M., and Kamo, S. L. (2012a). Origin of an unusual monazite-xenotime gneiss, Hudson Highlands, New York: SHRIMP U-Pb geochronology and trace element geochemistry. *Am. J. Sci.* 312, 723–765. doi: 10.2475/07.2012.02

Aleinikoff, J. N., Hayes, T. S., Evans, K. V., Mazdab, F. K., Pillers, R. M., and Fanning, C. M. (2012b). SHRIMP U-Pb ages of xenotime and monazite from the Spar Lake Red Bed-associated Cu-Ag deposit, Western Montana: implications for Ore Genesis. *Econ. Geol.* 107, 1251–1274. doi: 10.2113/econgeo.107.6.1251

Audren, C., and Triboulet, C. (1993). P-T-t-deformation paths recorded by kinzigites during diapirism in the western Variscan belt (Golfe du Morbihan, southern Brittany, France). *J. Metamorph. Geol.* 11, 337–356. doi: 10.1111/j.1525-1314.1993.tb00152.x

Ayers, J. C., Miller, C. F., Gorisch, B., and Milleman, J. (1999). Textural development of monazite during high-grade metamorphism: hydrothermal growth kinetics, with implications for U, Th-Pb geochronology. *Am. Mineral.* 84, 1766–1780. doi: 10.2138/am-1999-11-1206

Barbarin, B. (1998). A review of the relationships of granitoid types, their origins and their geodynamic environments. *Lithos* 46, 605–626. doi: 10.1016/s0024-4937(98)00085-1

Bea, F., and Montero, P. (1999). Behavior of accessory phase and redistribution of Zr, REE, Y, Th, and U during metamorphism and partial melting of metapelites in the lower crust: an example from the Kinzigite Formation of Ivrea-Verbano, NW Italy. *Geochim. Cosmochim. Acta* 63, 1133–1153. doi: 10.1016/s0016-7037(98)00292-0

Berger, A., Scherrer, N. C., and Bussi, F. (2005). Equilibration and disequilibration between monazite and garnet: indication from phase-composition and quantitative texture analysis. *J. Metamorph. Geol.* 2005, 865–880. doi: 10.1111/j.1525-1314.2005.00614.x

Bingen, B., Demaiffe, D., and Hertogen, J. (1996). Redistribution of rare earth elements, thorium, and uranium over accessory minerals in the course of amphibolite to granulite facies metamorphism; the role of apatite and monazite in orthogneisses from south western Norway. *Geochim. Cosmochim. Acta* 60, 1341–1354. doi: 10.1016/0016-7037(96)00006-3

Brandt, S., Schenk, V., Raith, M. M., Appel, P., Gerdes, A., and Srikantappa, C. (2011). Late Neoproterozoic P-T evolution of HP-UHT granulites from the Palni Hills (South India): new constraints from phase diagram modelling, LA-ICP-MS zircon dating and *in-situ* EMP monazite dating. *J. Petrol.* 52, 1813–1856. doi: 10.1093/petrology/egr032

Braun, I., Montel, J.-M., and Nicollet, C. (1998). Electron microprobe dating of monazites from high-grade gneisses and pegmatites of the Kerala Khondalite Belt, southern India. *Chem. Geol.* 146, 65–85. doi: 10.1016/s0009-2541(98)00005-9

Breithaupt, A. (1829). Über den Monazit, eine neue Specie des Mineral Reichs. *J. Chem. Phys.* 55, 301–303.

Broska, I., and Siman, P. (1998). The breakdown of monazite in the West-Capathian Veporic orthogneisses and Tatric granites. *Geol. Carpath.* 49, 161–167.

Budzyń, B., Harlov, D. E., Williams, M. L., and Jercinovic, M. J. (2011). Experimental determination of stability relations between monazite, fluorapatite, allanite, and REE-epidote as a function of pressure, temperature, and fluid composition. *Am. Mineral.* 96, 1547–1567. doi: 10.2138/am.2011.3741

Budzyń, B., Harlov, D. E., Kozub-Budzyń, G. A., and Majka, J. (2017). Experimental constraints on the relative stabilities of the two systems monazite-(Ce) – allanite-(Ce) – fluorapatite and xenotime-(Y) – (Y,HREE)-rich epidote – (Y,HREE)-rich fluorapatite, in high Ca and Na-Ca environments under P-T conditions of 200–1000 MPa and 450–750 °C. *Mineral. Petrol.* 111, 183–217. doi: 10.1007/s00710-016-0464-0

Cherniak, D. J., Watson, E. B., Grove, M., and Harrison, T. M. (2004). Pb diffusion in monazite: a combined RBS/SIMS study. *Geochim. Cosmochim. Acta* 68, 829–840. doi: 10.1016/j.gca.2003.07.012

Cocherie, A., Be Mézème, E., Legendre, O., Fanning, C. M., Faure, M., and Rossi, P. (2005). Electron microprobe dating as a tool for determining the closure of Th-U-Pb systems in migmatitic monazites. *Am. Mineral.* 90, 607–618. doi: 10.2138/am.2005.1303

Crowley, J. L., and Ghent, E. D. (1999). An electron microprobe study of the U-Pb-Th systematics in metamorphosed monazite: the role of Pb diffusion versus overgrowth and recrystallization. *Chem. Geol.* 157, 285–302. doi: 10.1016/s0009-2541(99)00009-1

Djouka-Fonkwe, M. L., Schulz, B., Schüssler, U., Tchouankoue, J.-P., and Nzolang, C. (2008). Geochemistry of the Bafoussam Pan-African I- and S-type granitoids in western Cameroon. *J. Afr. Earth Sci.* 50, 148–167. doi: 10.1016/j.jafrearsci.2007.09.015

England, P. C., and Thompson, A. B. (1984). Pressure-temperature-time paths of regional metamorphism. I. Heat transfer during the evolution of regions of thickened continental crust. *J. Petrol.* 25, 894–928. doi: 10.1093/petrology/25.4.894

Finger, F., and Krenn, E. (2007). Three metamorphic monazite generations in a high-pressure rock from the Bohemian Massif and the potentially important role of apatite in stimulating polyphase monazite growth along a PT loop. *Lithos* 95, 115–125.

Finger, F., Broska, I., Roberts, M. P., and Schermaier, A. (1998). Replacement of primary monazite by fluorapatite–allanite–epidote coronas in an amphibolite facies granite gneiss from the eastern Alps. *Am. Mineral.* 83, 248–258. doi: 10.2138/am-1998-3-408

Finger, F., Krenn, E., Riegler, G., Romano, S., and Zulauf, G. (2002). Resolving Cambrian, Carboniferous, Permian and Alpine monazite generations in the polymetamorphic basement of eastern Crete (Greece) by means of the electron microprobe. *Terra Nova* 14, 233–240. doi: 10.1046/j.1365-3121.2002.00415.x

Finger, F., Broska, I., Haunschmid, B., Hrasko, L., Kohut, M., Krenn, E., et al. (2003). Electron-microprobe dating of monazites from Western Carpathian basement granitoids: plutonic evidence for an important Permian rifting event subsequent to Variscan crustal anatexis. *Int. J. Earth Sci.* 92, 86–98. doi: 10.1007/s00531-002-0300-0

Finger, F., Krenn, E., Schulz, B., Harlov, D. E., and Schiller, D. (2016). Satellite monazites in polymetamorphic basement rocks of the Alps: their origin and

petrological significance. *Am. Mineral.* 101, 1094–1103. doi: 10.2138/am-2016-5477

Förster, H.-J. (1998). The chemical composition of REE-Y-Th-U-rich accessory minerals in peraluminous granites of the Erzgebirge-Fichtelgebirge region, Germany, Part I: the monazite-(Ce)-brabantite solid solution series. *Am. Mineral.* 83, 259–272. doi: 10.2138/am-1998-3-409

Foster, G., Parrish, R. R., Horstwood, M. S. A., Chenery, S., Pyle, J., and Gibson, H. D. (2004). The generation of prograde P–T–t points and paths; a textural, compositional, and chronological study of metamorphic monazite. *Earth Planet. Sci. Lett.* 228, 125–142. doi: 10.1016/j.epsl.2004.09.024

Franz, G., Andrehs, G., and Rhede, D. (1996). Crystal chemistry of monazite and xenotime from Saxothuringian-Moldanubian metapelites, NE Bavaria, Germany. *Eur. J. Mineral.* 8, 1097–1118. doi: 10.1127/ejm/8/5/1097

Frey, M., Desmons, J., and Neubauer, F. (1999). The new metamorphic map of the Alps. *Swiss Bull. Mineral. Petrol.* 79, 1–4. doi: 10.5382/rev.11.11

Gasser, D., Bruand, E., Rubatto, D., and Stüwe, K. (2012). The behaviour of monazite from greenschist facies phyllites to anatectic gneisses: an example from the Chugach Metamorphic Complex, southern Alaska. *Lithos* 13, 108–122. doi: 10.1016/j.lithos.2011.12.003

Grapes, R., Bucher, K., and Hoskin, P. W. O. (2005). Monazite-epidote reaction in amphibolite grade blackwall rocks. *Eur. J. Mineral.* 17, 553–566. doi: 10.1127/0935-1221/2005/0017-0553

Gratz, R., and Heinrich, W. (1997). Monazite–xenotime thermobarometry: experimental calibration of the miscibility gap in the binary system $CePO_4$-YPO_4. *Am. Mineral.* 82, 772–780. doi: 10.2138/am-1997-7-816

Harlov, D. E., and Förster, H. J. (2003). Fluid-induced nucleation of (Y+REE)-phosphate minerals within apatite: nature and experiment. Part II. Fluorapatite. *Am. Mineral.* 88, 1209–1229. doi: 10.2138/am-2003-8-905

Harlov, D. E., Wirth, R., and Förster, H. J. (2005). An experimental study of dissolution–reprecipitation in fluorapatite: fluid infiltration and the formation of monazite. *Contrib. Mineral. Petrol.* 150, 268–286. doi: 10.1007/s00410-005-0017-8

Harlov, D. E., Wirth, R., and Hetherington, C. J. (2011). Fluid-mediated partial alteration in monazite: the role of coupled dissolution–reprecipitation in element redistribution and mass transfer. *Contrib. Mineral. Petrol.* 162, 329–348. doi: 10.1007/s00410-010-0599-7

Harrison, T. M., Catlos, E. J., and Montel, J.-M. (2002). U–Th–Pb dating of phosphate minerals. *Rev. Mineral. Geochem.* 48, 524–558. doi: 10.2138/rmg.2002.48.14

Hawkins, D. P., and Bowring, S. A. (1999). U-Pb monazite, xenotime, and titanite geochronological constraints on the prograde to post-peak metamorphic thermal history of Paleoproterozoic migmatites from the Grand Canyon, Arizona. *Contrib. Mineral. Petrol.* 134, 150–169. doi: 10.1007/s004100050475

Hecht, L., and Cuney, M. (2000). Hydrothermal alteration of monazite in the Precambrian crystalline basement of the Athabasca Basin (Saskatchewan, Canada): implications for the formation of unconformity-related uranium deposits. *Mineral. Depos.* 35, 791–795. doi: 10.1007/s001260050280

Heinrich, W., Andrehs, G., and Franz, G. (1997). Monazite-xenotime miscibility gap thermometry. I. An empirical calibration. *J. Metamorph. Geol.* 15, 3–16. doi: 10.1111/j.1525-1314.1997.t01-1-00052.x

Hetherington, C. J., Harlov, D. E., and Budzyń, B. (2010). Experimental initiation of dissolution-reprecipitation reactions in monazite and xenotime: the role of fluid composition. *Mineral. Petrol.* 99, 165–184. doi: 10.1007/s00710-010-0110-1

Holland, T. J. B., and Powell, R. (1998). An internally-consistent thermodynamic dataset for phases of petrological interest. *J. Metamorph. Geol.* 16, 309–344. doi: 10.1111/j.1525-1314.1998.00140.x

Holland, T. J. B., and Powell, R. (2011). An improved and extended internally consistent thermodynamic dataset for phases of petrological interest, involving a new equation of state for solids. *J. Metamorph. Geol.* 29, 333–383. doi: 10.1111/j.1525-1314.2010.00923.x

Imayama, T., and Suzuki, K. (2013). Carboniferous inherited grain and age zoning of monazite and xenotime from leucogranites in far-eastern Nepal: constraints from electron probe microanalysis. *Am. Mineral.* 98, 1393–1406. doi: 10.2138/am.2013.4267

Janots, E., Brunet, F., Goffe, B., Poinssot, C., Burchard, M., and Cemic, L. (2007). Thermochemistry of monazite-(La) and dissakisite (La): implications for monazite and allanite stability in metapelites. *Contrib. Mineral. Petrol.* 154, 1–14. doi: 10.1007/s00410-006-0176-2

Janots, E., Engi, M., Berger, A., Allaz, J., Schwarz, J. O., and Spandler, C. (2008). Prograde metamorphic sequence of REE minerals in pelitic rocks of the Central Alps: implications for allanite–monazite–xenotime phase relations from 250 to 610 °C. *J. Metamorph. Geol* 26, 509–526. doi: 10.1111/j.1525-1314.2008.00774.x

Janots, E., Berger, A., Gnos, E., Whitehouse, M., Lewin, E., and Pettke, T. (2012). Constraints on fluid evolution during metamorphism from U–Th–Pb systematics in Alpine hydrothermal monazite. *Chem. Geol.* 32, 61–71. doi: 10.1016/j.chemgeo.2012.07.014

Jercinovic, M. J., Williams, M. L., and Lane, E. D. (2008). In-situ trace element analysis of monazite and other fine-grained accessory minerals by EPMA. *Chem. Geol.* 254, 197–215. doi: 10.1016/j.chemgeo.2008.05.016

Johan, Z., and Johan, V. (2005). Accessory minerals of the Cínovec (Zinnwald) granite cupola, Czech Republic: indicators of petrogenetic evolution. *Mineral. Petrol.* 83, 113–150. doi: 10.1007/s00710-004-0058-0

Johannes, W., and Holtz, F. (1996). *Petrogenesis and experimental petrology of granitic rocks*. Berlin: Springer-Verlag.

Just, J., Schulz, B., de Wall, H., Jourdan, F., and Pandit, M. K. (2010). Monazite CHIME/EPMA dating of Erinpura granitoid deformation: implications for Neoproterozoic tectono-thermal evolution of NW India. *Gondwana Res.* 19, 402–412. doi: 10.1016/j.gr.2010.08.002

Kelsey, D. E., Clark, C., and Hand, M. (2008). Thermobarometric moselling of zircon and monazite growth in melt-bearing systems: examples using model metapelitic and metapsammitic granulites. *J. Metamorph. Geol.* 26, 199–212. doi: 10.1111/j.1525-1314.2007.00757.x

Kempe, U., Lehmann, B., Wolf, D., Rodionov, N., Bombach, K., Schwengfelder, U., et al. (2008). U–Pb SHRIMP geochronology of Th-poor, hydrothermal monazite: an example from the Llallagua tin-porphyry deposit, Bolivia. *Geochim. Cosmochim. Acta* 72, 4352–4366. doi: 10.1016/j.gca.2008.05.059

Kerrick, D. M. (1972). Experimental determination of muscovite + quartz stability with $P_{H2O} < P_{Total}$. *Am. J. Sci.* 272, 946–958. doi: 10.2475/ajs.272.10.946

Krenn, E., Janak, M., Finger, F., Broska, I., and Koneèny, P. (2009). Two types of metamorphic monazite with contrasting La/Nd, Th, and Y signatures in an ultrahigh-pressure metapelite from the Pohorje Mountains, Slovenia: indications for pressure-dependent REE exchange between apatite and monazite? *Am. Mineral.* 94, 801–815. doi: 10.2138/am.2009.2981

Krenn, E., Schulz, B., and Finger, F. (2012). Three generations of monazite in Austroalpine basement rocks to the south of the Tauern Window - evidences for Variscan, Permian and Alpine metamorphism. *Swiss J. Geosci.* 105, 1–18. doi: 10.1007/s00015-012-0104-6

Lee, D. E., and Bastron, H. (1967). Fractionation of rare-earth elements in allanite and monazite as related to geology of the Mt. Wheeler mine area, Nevada. *Geochim. Cosmochim. Acta* 31, 339–356. doi: 10.1016/0016-7037(67)90046-4

Lee, D. E., and Dodge, F. C. W. (1964). Accessory minerals in some granitic rocks in California and Nevada as a function of calcium content. *Am. Mineral.* 49, 1660–1669.

Ling, X.-X., Huyskens, M. H., Li, Q. L., Yin, Q.-Z., Werner, R., Liu, Y., et al. (2017). Monazite RW-1: a homogenous natural reference material for SIMS U–Pb and Th–Pb isotopic analysis. *Mineral. Petrol.* 111, 163–172. doi: 10.1007/s00710-016-0478-7

Linthout, K. (2007). Tripartite division of the system $2REEPO_4$ – $CaTh(PO_4)_2$ – $2ThSiO_4$, discreditation of brabantite, and recognition of cheralite as the name for members dominated by $CaTh(PO_4)_2$. *Can. Mineral.* 45, 503–508. doi: 10.2113/gscanmin.45.3.503

Lopez de Luchi, M., Martinez Dopico, C. I., Cutts, K., Schulz, B., Montenegro, T., Siegesmund, S., et al. (2020). The Conlara metamorphic complex: lithology, provenance, metamorphic constraints on the metabasic rocks and CHIME monazite dating. *J. South Am. Earth Sci.* 106:103065. doi: 10.1016/j.jsames.2020.103065

Massonne, H.-J. (2003). A comparison of the evolution of diamondiferous quartz-rich rocks from the Saxonian Erzgebirge and the Kokchetav Massif: are so-called diamondiferous gneisses magmatic rocks? *Earth Planet. Sci. Lett.* 216, 345–362.

Meldrum, A., Boatner, L. A., Weber, W. J., and Ewing, R. C. (1998). Radiation damage in zircon and monazite. *Geochim. Cosmochim. Acta* 62, 2509–2520. doi: 10.1016/s0016-7037(98)00174-4

Mingram, B., and Rötzler, K. (1999). Geochemische, petrologische und geochronologische Untersuchungen im Erzgebirgskristallin: rekonstruktion

eines Krustenstapels. *Schriftenreihe für Geowissenschaften* 9, 1–80. (Gesellschaft für Geowissenschaften).

Montel, J.-M. (1993). A model for monazite/melt equilibrium and application to the generation of granitic magmas. *Chem. Geol.* 110, 127–146. doi: 10.1016/0009-2541(93)90250-m

Montel, J., Foret, S., Veschambre, M., Nicollet, C., and Provost, A. (1996). A fast, reliable, inexpensive in-situ dating technique: electron microprobe ages on monazite. *Chem. Geol.* 131, 37–53.

Montel, J.-M., Kato, T., Enami, M., Cocherie, A., Finger, F., Williams, M. L., et al. (2018). Electron-microprobe dating of monazite: the story. *Chem. Geol.* 484, 4–15. doi: 10.1016/j.chemgeo.2017.11.001

Mottrama, C. M., Warrena, C. W., Regisa, D., Roberts, N. M. W., Harris, N. B. W., Arglesa, T. W., et al. (2014). Developing an inverted Barrovian sequence; insights from monazite petrochronology. *Earth Planet. Sci. Lett.* 403, 418–431. doi: 10.1016/j.epsl.2014.07.006

Nasdala, L., Akhmadaliev, S., Artac, A., Chanmuang, N. C., Habler, G., and Lenz, C. (2018). Irradiation effects in monazite–(Ce) and zircon: raman and photoluminescence study of Au-irradiated FIB foils. *Phys. Chem. Mineral.* 45, 855–871. doi: 10.1007/s00269-018-0975-9

Ondrejka, M., Uher, P., Pršek, J., and Ozdín, D. (2007). Arsenian monazite-(Ce) and xenotime-(Y), REE arsenates and carbonates from the Tisovec-Rejkovo rhyolite, Western Carpathians, Slovakia: composition and substitutions in the $(REE,Y)XO_4$ system (X = P, As, Si, Nb, S). *Lithos* 95, 116–129. doi: 10.1016/j.lithos.2006.07.019

Ondrejka, M., Uher, P., and Konečný, P. (2009). Magmatic and post-magmatic Y-REE-Th phosphate, silicate and Nb–Ta-Y-REE oxide minerals in A-type metagranite: an example from the Turèok massif, the Western Carpathians, Slovakia. *Min. Mag.* 73, 1009–1025. doi: 10.1180/minmag.2009.073.6.1009

Ondrejka, M., Uher, P., Putis, M., Broska, I., Bacik, P., and Koneènı, P. (2012). Two-stage breakdown of monazite by post-magmatic and metamorphic fluids: an example from the Veporic orthogneiss, Western Carpathians, Slovakia. *Lithos* 14, 245–255. doi: 10.1016/j.lithos.2012.03.012

Oriolo, S., Wemmer, K., Oyhantçabal, P., Fossen, H., Schulz, B., and Siegesmund, S. (2018). Geochronology of shear zones - A review. *Earth Sci. Rev.* 185, 665–683. doi: 10.1016/j.earscirev.2018.07.00

Oriolo, S., Schulz, B., González, P. D., Bechis, F., Olaizola, E., Krause, J., et al. (2019). The Late Paleozoic tectonometamorphic evolution of Patagonia revisited: insights from the pressure-temperature-deformation-time (P-T-D-t) path of the Gondwanide basement of the North Patagonian Cordillera (Argentina). *Tectonics* 38, 2378–2400. doi: 10.1029/2018TC005358

Overstreet, W. C. (1967). The geologic occurrence of monazite. *U. S. Geol. Surv. Prof. Paper* 530:327.

Oyhantçabal, P., Eimer, M., Wemmer, K., Schulz, B., Frei, R., and Siegesmund, S. (2012). Paleo- and Neoproterozoic magmatic and tectonometamorphic evolution of the Isla Cristalina de Rivera (Nico Pérez Terrane, Uruguay). *Int. J. Earth Sci.* 101, 1745–1762. doi: 10.1007/s00531-012-0757-4

Parrish, R. R. (1990). U-Pb dating of monazite and its application to geological problems. *Can. J. Earth Sci.* 27, 1431–1450. doi: 10.1139/e90-152

Passchier, C. W., and Trouw, R. A. J. (2005). *Microtectonics*, 2nd Edn. Heidelberg: Springer, 289.

Petrík, I., Janák, M., Klonowska, I., Maika, J., Froitzheim, N., Yoshida, K., et al. (2019). Monazite behaviour during metamorphic evolution of a diamond-bearing gneiss: a case study from the Seve Nappe Complex, Scandinavian Caledonides. *J. Petrol.* 60, 1773–1796.

Poitrasson, F., Chenery, S. R., and Bland, D. J. (1996). Contrasted monazite hydrothermal alteration mechanisms and their geochemical implications. *Earth Planet. Sci. Lett.* 145, 79–96. doi: 10.1016/s0012-821x(96)00193-8

Powell, R., and Holland, T. J. B. (1994). Optimal geothermometry and geobarometry. *Am. Mineral.* 79, 120–133.

Powell, R., and Holland, T. J. B. (2008). On thermobarometry. *J. Metamorph. Geol.* 26, 155–179.

Pyle, J. M., and Spear, F. S. (2003). Four generations of accessory-phase growth in low-pressure migmatites from SW New Hampshire. *Am. Mineral.* 88, 338–351. doi: 10.2138/am-2003-2-311

Pyle, J. M., Spear, F. S., Rudnick, R. L., and McDonough, W. F. (2001). Monazite-xenotime-garnet equilibrium in metapelites and a new monazite-garnet thermometer. *J. Petrol.* 42, 2083–2107. doi: 10.1093/petrology/42.11.2083

Pyle, J. M., Spear, F. S., and Wark, D. A. (2002). Electron microprobe analysis of REE in apatite, monazite, and xenotime: protocols and pitfalls. *Rev. Mineral. Geochem.* 48, 337–362. doi: 10.2138/rmg.2002.48.8

Pyle, J. M., Spear, F. S., Cheney, J. T., and Layne, G. (2005). Monazite ages in the Chesham Pond Nappe, SW New Hampshire, USA: implications for assembly of central New England thrust sheets. *Am. Mineral.* 90, 592–606. doi: 10.2138/am.2005.1341

Quarton, M., Zouiri, M., and Freundlich, W. (1994). Cristallochimie des orthophosphates doubles de thorium et de plomb. *Compt. Rend. Acad. Sci. Paris* 229, 785–788.

Read, D., Andreoly, M. A. G., Knoper, M., Williams, C. T., and Javris, N. (2002). The degradation of monazite: implications for the mobility of rare-earth and actinide elements during low-temperature alteration. *Eur. J. Mineral.* 14, 487–498. doi: 10.1127/0935-1221/2002/0014-0487

Richter, M., Nebel-Jacobsen, Y., Nebel, O., Zack, T., Mertz-Kraus, R., Raveggi, M., et al. (2019). Assessment of five monazite reference materials for U-Th/Pb dating using laser-ablation ICP-MS. *Geosciences* 201:391. doi: 10.3390/geosciences9090391

Rode, S., Rösel, D., and Schulz, B. (2012). Constraints on the Variscan P-T evolution by EMP Th-U-Pb monazite dating in the polymetamorphic Austroalpine Oetztal-Stubai basement (Eastern Alps). *Zeitschr. Dt. Ges. Geowiss.* 163, 43–67. doi: 10.1127/1860-1804/2012/0163-0043

Rubatto, D., Williams, I. S., and Buick, I. S. (2001). Zircon and monazite response to prograde metamorphismin the Reynolds Range, central Australia. *Contrib. Mineral. Petrol.* 140, 458–468. doi: 10.1007/pl00007673

Schandl, E., and Gorton, M. P. (2004). A textural and geochemical guide to the identification of hydrothermal monazite: criteria for selection of samples for dating epigenetic hydrothermal ore deposits. *Econ. Geol.* 99, 1027–1035. doi: 10.2113/gsecongeo.99.5.1027

Scherrer, N. C., Engi, M., Gnos, E., Jakob, V., and Leichti, A. (2000). Monazite analysis; from sample preparation to microprobe age dating and REE quantification. *Swiss Bull. Mineral. Petrol.* 80, 93–105.

Schulz, B. (2010). Geothermobarometrische Analysen und Monazit-Altersdatierung an einem Hercynit-Sillimanit-Cordierit-Granat-Gneis (Moldanubikum des Oberpfälzer Waldes bei Weiding. *Geol. Bl.* 59, 239–256.

Schulz, B. (2013). Monazite EMP-Th-U-Pb age pattern in Variscan metamorphic units in the Armorican Massif (Brittany, France). *Zeitschr. dt. Ges. Geowiss.* 164, 313–335. doi: 10.1127/1860-1804/213/0008

Schulz, B. (2014). Early Carboniferous P–T path from the Upper Gneiss Unit of Haut-Allier (French Massif Central) – reconstructed by geothermobarometry and EMP–Th–U–Pb monazite dating. *J. Geosci.* 59, 327–349. doi: 10.3190/jgeosci

Schulz, B. (2017). Polymetamorphism in garnet micaschists of the Saualpe Eclogite Unit (Eastern Alps, Austria), resolved by automated SEM methods and EMP-Th-U-Pb monazite dating. *J. Metamorphic Geol.* 3, 141–163. doi: 10.1111/jmg.12224

Schulz, B., and von Raumer, J. F. (2011). Discovery of Ordovician-Silurian metamorphic monazite in garnet metapelites of the Alpine External Aiguilles Rouges Massif. *Swiss J. Geosci.* 104, 67–79. doi: 10.1007/s00015-010-0048-7

Schulz, B., and Schüssler, U. (2013). Electron-microprobe Th-U-Pb monazite dating in Early-Paleozoic high-grade gneisses as a completion of U-Pb isotopic ages (Wilson Terrane, Antarctica). *Lithos* 17, 178–192. doi: 10.1016/j.lithos.2013.05.008

Schulz, B., and Krause, J. (2018). Petrochronology of kinzigites in the Variscan Saxonian Granulite Massif by electron microprobe analysis and electron microscopy. *GeoBonn* 2018, Abstracts,A–241.

Schulz, B., and Krause, J. (2021). Electron probe petrochronology of polymetamorphic garnet micaschists in the lower nappe units of the Austroalpine Saualpe basement (Carinthia, Austria). *Zeitschr. Dt. Ges. Geowiss* 172/1. doi: 10.1127/zdgg/2021/0247

Schulz, B., Krenn, E., Finger, F., Brätz, H., and Klemd, R. (2007). Cadomian and Variscan metamorphic events in the Léon Domain (Armorican Massif, France): P-T data and EMP monazite dating. In: U. Linnemann, D. Nance, P. Kraft, and G. Zulauf (Eds). *The Evolution of the Rheic Ocean: From Avalonian-Cadomian active margin to Alleghenian-Variscan collision*, (USA: Geological Society of America).

Schulz, B., Krause, J., and Schüssler, U. (2017). Electron microprobe Th-U-Pb monazite dating of Devonian metamorphism in Münchberg and Frankenberg

allochthonous units in the Saxothuringian Zone. *GeoBremen* 2017, Abstracts,A–241.

Schulz, B., Krause, J., and Zimmermann, R. (2019b). Electron microprobe petrochronology of monazite-bearing garnet micaschists in the Oetztal-Stubai Complex (Alpeiner Valley, Stubai). *Swiss J. Geosci.* 112, 597–617. doi: 10.1007/s00015-019-00351-4(0)

Schulz, B., Krause, J., and Lapp, M. (2019a). Petrochronology by EPMA and automated SEM in the Saxothuringian high pressure nappes of the central and western Erzgebirge. *GeoMuenster* 2019, Abstracts,74.

Schulz, B., Sandmann, D., and Gilbricht, S. (2020). SEM-based Automated Mineralogy and its Application in Geo- and Material Sciences. *Minerals* 10:1004. doi: 10.3390/min10111004

Seydoux-Guillaume, A.-M., Montel, J.-M., Bingen, B., Bosse, V., de Parseval, P., Paquette, J.-L., et al. (2012). Low-temperature alteration of monazite: fluid mediated coupled dissolution-precipitation, irradiation damage, and disturbance of the U/Pb and Th/Pb chronometers. *Chem. Geol.* 33, 140–158. doi: 10.1016/j.chemgeo.2012.07.031

Simmat, R., and Raith, M. M. (2008). U–Th–Pb monazite geochronometry of the Eastern Ghats Belt, India: timing and spatial disposition of poly-metamorphism. *Precambrian Res.* 162, 16–39. doi: 10.1016/j.precamres.2007.07.016

Skrzypek, E., Sakata, S., and Sorger, D. (2020). Alteration of magmatic monazite in granitoids from the Ryoke belt (SW Japan): processes and consequences. *Am. Mineral.* 105, 538–554. doi: 10.2138/am-2020-7025

Spear, F. S. (1993). "Metamorphic phase equilibria and pressure-temperature-time paths," in *Mineralogical Society of America Monography*, (Virginia, U.S: Mineralogical Society of America),

Spear, F. S. (2010). Monazite-allanite phase relations in metapelites. *Chem. Geol.* 279, 55–62. doi: 10.1016/j.chemgeo.2010.10.004

Spear, F. S., and Pyle, J. M. (2002). Apatite, monazite and xenotime in metamorphic rocks. *Rev. Mineral. Geochem.* 48, 293–335. doi: 10.1515/9781501509636-010

Spear, F. S., and Pyle, J. M. (2010). Theoretical modeling of monazite growth in a low-Ca metapelite. *Chem. Geol.* 273, 111–119. doi: 10.1016/j.chemgeo.2010.02.016

Spear, F. S., Pyle, J. M., and Cherniak, D. (2009). Limitations of chemical dating of monazite. *Chem. Geol.* 266, 218–230. doi: 10.1016/j.chemgeo.2009.06.007

Suzuki, K., and Adachi, M. (1991). Precambrian provenance and Silurian metamorphism of the Tsunosawa paragneiss in the South Kitakami terrane, Northeast Japan, revealed by the chemical Th-U-total Pb isochron ages of monazite, zircon and xenotime. *Geochem. J.* 25, 357–376. doi: 10.2343/geochemj.25.357

Suzuki, K., and Kato, T. (2008). CHIME dating of monazite, xenotime, zircon and polycrase: protocol, pitfalls and chemical criterion of possible discordant age data. *Gondwana Res.* 14, 569–586. doi: 10.1016/j.gr.2008.01.005

Tchato, D. T., Schulz, B., and Nzenti, P. (2009). Electron microprobe dating and thermobarometry of Neoproterozoic metamorphic events in the Kekem area, Central African Fold Belt of Cameroon. *Neues Jahrb. Geol. Palaontol. Abh.* 18, 95–109. doi: 10.1127/0077-7757/2009/0140

Thompson, A. B., and England, P. C. (1984). Pressure-temperature-time paths of regional metamorphism II. Their inference and interpretation using mineral assemblages in metamorphic rocks. *J. Petrol.* 25, 929–955. doi: 10.1093/petrology/25.4.929

Thöni, M. (1999). A review of geochronological data from the Eastern Alps. *Swiss J. Geosci. Suppl.* 79, 209–230.

Thöni, M., Miller, C., Blichert-Toft, J., Whitehouse, M. J., Konzett, J., and Zanetti, A. (2008). Timing of high-pressure metamorphism and exhumation of the eclogite type-locality (Kupplerbrunn-Prickler Halt, Saualpe, south-eastern Austria): constraints from correlations of the Sm-Nd, Lu-Hf, U-Pb and Rb-Sr isotopic systems. *J. Metamorph. Geol.* 26, 561–581. doi: 10.1111/j.1525-1314.2008.00778.x

Thöny, W. F., Tropper, P., Schennach, F., Krenn, E., Finger, F., Kaindl, R., et al. (2008). The metamorphic evolution of migmatites from the Ötztal Complex (Tyrol, Austria) and constraints on the timing of the pre-Variscan high-T event in the Eastern Alps. *Swiss J. Geosci.* 101, 111–126. doi: 10.1007/s00015-008-1290-0

Tichomirowa, M., Whitehouse, M., Gerdes, A., and Schulz, B. (2018). Zircon (Hf, O isotopes) as melt indicator: melt infiltration and abundant new zircon growth within melt rich layers of granulite-facies lenses versus solid-state recrystallization in hosting amphibolite-facies gneisses (central Erzgebirge, Bohemian Massif). *Lithos* 302–303, 65–85. doi: 10.1016/j.lithos.2017.12.020

Townsend, K. J., Miller, C. G., D'Andrea, J. L., Ayers, J. C., Harrison, T. M., and Coath, C. D. (2000). Low temperature replacement of monazite in the Ireteba granite, Southern Nevada: geochronological implications. *Chem. Geol.* 172, 95–112. doi: 10.1016/s0009-2541(00)00238-2

Upadhyay, D., and Pruseth, K. L. (2012). Fluid-induced dissolution breakdown of monazite from Tso Morari complex, NW Himalayas: evidence for immobility of trace elements. *Contrib. Mineral. Petrol.* 164, 303–316. doi: 10.1007/s00410-012-0739-3

Varga, J., Raimondo, T., Daczko, N. R., and Adam, J. (2020). Experimental alteration of monazite in granitic melt: variable U–Th–Pb and REE mobility during melt-mediated coupled dissolution-precipitation. *Chem. Geol.* 544:119602. doi: 10.1016/j.chemgeo.2020.119602

Watt, G. L., and Harley, S. L. (1993). Accessory phase controls on the geochemistry of crustal melts and restites produced during water-undersaturated partial melting. *Contrib. Mineral. Petrol.* 114, 550–566. doi: 10.1007/bf00321759

Wawrzenitz, N., Krohe, A., Rhede, D., and Romer, R. L. (2012). Dating rock deformation with monazite: the impact of dissolution precipitation creep. *Lithos* 13, 52–74. doi: 10.1016/j.lithos.2011.11.025

Williams, M. L., Jercinovic, M. J., and Terry, M. (1999). High resolution "age" mapping, chemical analysis, and chemical dating of monazite using the electron microprobe: a new tool for tectonic analysis. *Geology* 27, 1023–1026. doi: 10.1130/0091-7613(1999)027<1023:amadom>2.3.co;2

Williams, M. L., Jercinovic, M. J., Harlov, D. E., Budzyń, B., and Hetherington, C. J. (2011). Resetting monazite ages during fluid-related alteration. *Chem. Geol.* 283, 218–225. doi: 10.1016/j.chemgeo.2011.01.019

Williams, M. L., Jercinovic, M. J., Mahan, K. H., and Dumond, G. (2017). Electron Microprobe Petrochronology. *Rev. Mineral. Geochem.* 83, 153–182. doi: 10.1515/9783110561890-006

Willner, A. P., Krohe, A., and Maresch, W. V. (2000). Interrelated P-T-t-d paths in the Variscan Erzgebirge dome (Saxony, Germany): constraints on the rapid exhumation of high-pressure rocks from the root zone of a collisional orogen. *Int. Geol. Rev.* 42, 64–85. doi: 10.1080/00206810009465070

Wing, B. A., Ferry, J. M., and Harrison, T. M. (2003). Prograde destruction and formation of monazite and allanite during contact and regional metamorphism of pelites: petrology and geochronology. *Contrib. Mineral. Petrol.* 145, 228–250. doi: 10.1007/s00410-003-0446-1

Yakymchuk, C. (2017). Behaviour of apatite during partial melting of metapelites and consequences for prograde suprasolidus monazite growth. *Lithos* 274-275, 412–426. doi: 10.1016/j.lithos.2017.01.009

Zeh, A., Williams, I. S., Brätz, H., and Millar, I. L. (2003). Different age response of zircon and monazite during the tectonometamorphic evolution of a high-grade paragneiss from the Ruhla Crystalline Complex, central Germany. *Contrib. Mineral. Petrol.* 145, 691–706. doi: 10.1007/s00410-003-0462-1

Zhang, Y. B., Li, Q. L., Lan, Z. W., Wu, F. Y., Li, X. H., Yang, J. H., et al. (2015). Diagenetic xenotime dating to constrain the initial depositional time of the Yan–Liao rift. *Precambrian Res.* 271, 20–32. doi: 10.1016/j.precamres.2015.09.024

Zhu, X. K., and O'Nions, R. K. (1999). Zonation of monazite in metamorphic rocks and its implications for high temperature thermochronology: a case study from the Lewisian terrain. *Earth Planet. Sci. Lett.* 171, 209–220. doi: 10.1016/s0012-821x(99)00146-6

Conflict of Interest: The author declares that the research was conducted in the absence of any commercial or financial relationships that could be construed as a potential conflict of interest.